Ceramic Acoustic Horns

Emil Degerth

DIVISION OF INNOVATION | DEPARTMENT OF DESIGN SCIENCES
FACULTY OF ENGINEERING LTH | LUND UNIVERSITY

2026

BACHELOR THESIS

Ceramic Acoustic Horns

Design, Fabrication, and Acoustical Study

Emil Degerth

Ceramic Acoustic Horns

Design, Fabrication, and Acoustical Study

Published by
Department of Design Sciences
Faculty of Engineering LTH, Lund University
P.O. Box 118, SE-221 00 Lund, Sweden

Subject: Technical Design (MMKL05)

Division: Innovation

Supervisor: Jože Tavčar

Co-supervisor: Olof Jansson

Co-supervisor: Tsvetan Ewald (Arda Audio)

Examiner: Elin Olander

Abstract

This thesis documents the design and fabrication of ceramic loudspeaker horns using slip casting and digital fabrication tools, and evaluates their acoustic performance against geometrically equivalent 3D printed PLA reference horns. Two horn profiles were developed and realised through a workflow combining mathematical profile generation, CAD modelling, 3D printing, and slip casting.

The acoustic evaluation measured on-axis and off-axis frequency response and total harmonic distortion for all four horn configurations. Results showed that horn geometry exerted a substantially greater influence on acoustic behaviour than horn material. Differences between ceramic and PLA variants were small and largely fell within measurement uncertainty.

The manufacturing process proved to be the more complex outcome of the project. Ceramics is an unforgiving material that requires significant initial experimentation before consistent results can be achieved, and this thesis documents one part of that process. What the work demonstrates is that small-scale ceramic horn manufacturing is feasible, and that the case for ceramic as a horn material rests not entirely on acoustic performance advantages but on the surface character, visual weight, and sense of permanence that the material offers.

Keywords: acoustic horn, ceramic, slip casting, digital fabrication, small-scale manufacturing

Sammanfattning

Detta examensarbete dokumenterar design och tillverkning av keramiska högtalarhorn med hjälp av slamgjutning och digitala fabrikationsverktyg, samt utvärderar deras akustiska prestanda i jämförelse med geometriskt ekvivalenta referenshorn tillverkade i 3D printat PLA. Två hornprofiler utvecklades och realiserades genom ett arbetsflöde som kombinerar matematisk profilgenerering, CAD-modellering, 3D printning och slamgjutning.

Den akustiska utvärderingen, genomförd i ett ekofritt rum, mätte on-axis och off-axis frekvensrespons samt total harmonisk distorsion för alla fyra hornkonfigurationer. Resultaten visade att hornets geometri hade ett betydligt större inflytande på det akustiska beteendet än hornets material. Skillnaderna mellan keramiska och PLA-varianter var små och föll i de flesta fall inom mätosäkerheten.

Tillverkningsprocessen visade sig vara det mer komplexa utfallet av projektet. Keramik är ett krävande material som kräver betydande inledande experimentation innan konsekventa resultat kan uppnås, och detta examensarbete dokumenterar en del av den processen. Det arbetsflöde som utvecklats visar att småskalig tillverkning av keramiska horn är genomförbar, och att argumentet för keramik som hornmaterial inte vilar på akustiska prestandafördelar utan på den ytkaraktär, visuella tyngd och beständighet som materialet erbjuder.

Nyckelord: akustiskt horn, keramik, slamgjutning, digital fabrikation, småskalig tillverkning

Acknowledgments

I would like to thank my supervisor Jože for his guidance throughout this project, particularly with the engineering and physics aspects of the work.

A special thanks to Olof for his invaluable help in the ceramics studio and for his broader guidance on design practice. This project would not have been possible without his expertise and generosity with his time.

Thank you to Tsvetan at Arda Audio for allowing me to use it as a case study and for taking the time to discuss the project throughout its development.

Finally, I would like to thank the Lund University Humanities Lab for granting access to the anechoic chamber, which made the acoustic evaluation possible.

Lund, June 2026

Emil Degerth

Contents

1 Introduction

1.1 Background and Motivation

Since the early twentieth century, acoustic horns have remained a distinctive part of loudspeaker design [1]. Over time, the loudspeaker and the horn with it has grown from a device that simply reproduces sound, to an object in which engineering, craftsmanship, and artistic expression converge. Beyond their technical function, loudspeakers have found an important place in contemporary culture. They shape how music is experienced in homes, concert venues, and public spaces, and in some contexts they have become cultural artefacts in their own right. The sculptural nature of horns make them visually expressive objects, while their performance still strongly depends on precise engineering. Designing a horn therefore requires both technical understanding and sensitivity to form. The horn becomes a meeting point between acoustics and design.

Historically, horns have been manufactured from materials such as wood, metal, fibreglass composites, and plastics. In recent years, 3D printing has made it possible to produce complex horn geometries quickly and at relatively low cost. This illustrates how digital design and manufacturing tools have helped lower the barriers to entry for small-scale product development, allowing small studios to create highly customized products that previously required industrial manufacturing.

One such example is Arda Audio, a Copenhagen-based loudspeaker manufacturer whose products often centre around custom 3D printed horns. Through discussions with the founder Tsvetan, it became clear that rapid prototyping and design flexibility are central to enabling a small workshop like his to develop products that combine acoustic performance with a strong and recognizable visual identity. The autonomy that a small studio like his experiences when designing and producing highly specialised products with limited resources would have been difficult to achieve only a few decades ago. That said, these tools do not exist outside of the larger economic systems they emerged from. The machines, materials, and software remain largely owned and controlled by major corporations, and independent designers operate within that reality rather than outside it.

This perspective also relates to broader questions of sustainability. By reducing the need for dedicated industrial tooling and enabling production in smaller batches, digital fabrication can support more flexible and potentially more resource-conscious approaches to manufacturing. It suggests that designers and engineers can play a role in creating production systems that prioritize experimentation, repairibility, and aesthetic value rather than solely cost optimization.

Ceramic horns are rare and most often found in niche products produced by specialised ceramicists. However, the material offers qualities that make it particularly attractive for investigation. Fired ceramics are significantly stiffer than common thermoplastics and exhibit high surface hardness. In principle, this should make ceramic horns behave more closely to the rigid-wall assumptions commonly used in horn acoustics theory. At the same time, their compatibility with moulding methods allows them to be combined with modern digital tools, potentially offering a highly viable alternative to traditional manufacturing methods while still maintaining a level of scalability not easily reproducible with 3D printing alone.

Nevertheless, designing for a specific material introduces constraints. In cast ceramics, shrinkage, drying behaviour, and mould release all impose limitations that directly shape the final form. Rather than restricting the design, these constraints can result in creative solutions that may not have been explored otherwise. As Ulrich and Eppinger note, well-defined constraints can enhance innovation by narrowing the solution space and forcing more focused decisions [2]. This project applies that principle by treating the physical limitations of ceramics as a framework for the design process.

1.2 Aim and Research Questions

The project began with curiosity about whether ceramic horns could offer both unique aesthetic qualities and measurable acoustic benefits. As the work progressed, it became clear that the project was equally about developing a manufacturing process and understanding how a traditional craft material could be integrated into a contemporary product development workflow, thereby exploring what the design process looks like when engineering, craft, and manufacturing are treated as one continuous activity. The ceramic horn became both a product and a vehicle for investigating an alternative mode of making.

As such, this thesis is situated at the intersection of design and engineering, exploring how mathematical modelling, CAD, ceramics processing, prototyping, and acoustic testing can be combined in a single design process. It does not aim to provide a comprehensive guide to horn loudspeaker design; rather, it documents an exploratory, material-driven process where the manufacturing workflow is treated as an equally important outcome to the finished horn.

Consequently, the primary aim of the project is twofold:

1. To develop and document a feasible process for designing and manufacturing ceramic loudspeaker horns using slip casting and digital fabrication tools.
2. To investigate whether ceramic horns exhibit measurable acoustic differences compared with 3D-printed PLA horns of identical geometry.

1.2.1 Research Questions

To achieve these aims, the following research questions guide the work:

1. What design and manufacturing process is required to realise a ceramic loudspeaker horn?
2. Is this process technically feasible for small-scale production?
3. Does horn material (ceramic versus 3D-printed PLA) produce measurable differences in acoustic performance?

1.3 Scope

To maintain a manageable project scope within the timeframe of a bachelor's thesis, several boundaries were established.

While two distinct geometric profiles are utilized to gather comparative data, the acoustic optimization of these horn geometries is outside the scope of this work. Parameter selection is instead guided by established design practices, fabrication constraints, and aesthetic judgment.

Regarding the manufacturing workflow, the investigation is limited to a small selection of clay bodies and glaze systems. The process development focuses on identifying practical improvements, but does not evaluate production economics or establish a finalized system for commercial manufacturing.

Additionally, the evaluation is strictly based on objective, reproducible acoustic measurements and direct observations from the fabrication process. The thesis aims to provide a small exploratory foundation for combining digital tools with traditional ceramics, rather than a definitive characterization of all ceramic horn variables.

Finally, the manufacturing workflow was developed through a practice-based process, reflecting the author's personal exploration and development. While a background in traditional ceramics informed the material handling, the author had no prior experience combining digital manufacturing with slip casting at the outset. The final workflow was therefore shaped as much by material constraints as by a singular author's learning trajectory within the project's timeframe.

1.4 Relevance for Sustainable Development

The process developed in this thesis tries to align with sustainable development principles by exploring alternatives to centralised, high-volume mass production. By utilising digital fabrication to produce mould tooling, the process lowers the financial and material barriers to entry for small-scale, localised manufacturing. This decentralised approach reduces the environmental impacts associated with mass transportation and overproduction, while shifting the focus toward intentional, community-scale making.

Furthermore, the material choices and process design support resource efficiency. While digital fabrication often relies on synthetic polymers, using 3D printing primarily for mould making rather than the final product limits the amount of waste generated. Crucially, these 3D prints offer the benefit of being almost infinitely reusable for casting subsequent plaster moulds of the same design. Significant research is currently being allocated into making 3D printing filaments more sustainable and biodegradable; though these material systems are not yet completely circular, utilising them as a small, foundational part of a workflow that outputs a natural material like clay may reduce the overall environmental footprint. Ceramics themselves are derived from naturally abundant, geologically low-impact raw materials, providing a highly stable, inert medium for the final object. On a manufacturing level, integrating these digital workflows into the mould-making process allows for precise material calculation, minimising overall workshop waste.

This convergence of digital tools and traditional craft also preserves a meaningful connection between the object, the maker, and the user. By moving away from anonymous, mass-produced commodities toward a visible, understood manufacturing workflow, the project supports a culture of care and emotional durability, prioritising product longevity and craftsmanship over short consumption cycles. While it must be acknowledged that digital fabrication infrastructure itself still relies on global, corporate supply chains for machinery and software, utilising these tools to establish a localised ceramic practice represents a pragmatic step toward shifting where the final, physical value is created and retained.

It should be noted however that no formal life cycle assessment (LCA) was conducted as part of this project. While the use of ceramics and small-scale digital fabrication may offer certain environmental advantages, a complete assessment would need to consider factors such as energy consumption during firing, material sourcing, transportation, equipment manufacture, and end-of-life management.

1.5 Outline of the Thesis

This thesis combines a design and fabrication process with a controlled acoustic experiment. The overall structure follows a modified IMRaD convention (Introduction, Methodology, Results, and Discussion), with the results chapter organised around the phases of concept development, detailed design, and concept realisation, adapted from Ulrich and Eppinger [2].

The thesis is structured as follows:

- **Chapter 2 – Theory:** Presents the theoretical background on oscillating systems, horn acoustics, and ceramic slip casting.
- **Chapter 3 – Methodology:** Presents the methodological approach

underpinning the design, manufacturing, and acoustic evaluation.

- **Chapter 4 – Concept Development:** Describes the early ideation process and the selection of horn profiles and overall design direction.
- **Chapter 5 – Detailed Design:** Covers the mathematical parameterisation of the selected horn profiles and the CAD design of the horns and plaster moulds.
- **Chapter 6 – Concept Realisation:** Documents the manufacturing of the plaster moulds, slip-cast ceramic horns, and 3D-printed reference horns.
- **Chapter 7 – Acoustical Evaluation:** Presents the experimental setup and measurement methodology used to compare the horns, followed by the presentation and interpretation of the results.
- **Chapter 8 – Discussion:** Evaluates the findings from both the design process and the acoustic evaluation, contextualising the results within a wider design framework.
- **Chapter 9 – Conclusions:** Answers the research questions and suggests directions for future work.

2 Theory

To successfully develop digitally fabricated ceramic acoustic horns, insights from acoustic engineering, geometry generation, and material science must be synchronised. This chapter outlines the fundamental acoustic parameters of horn loudspeakers, the mathematics underpinning their geometries, and the physical constraints of ceramic manufacturing. These elements combined form the analytical baseline used to guide the development and evaluation of the physical prototypes.

Crucially, these three areas, acoustics, horn geometry, and ceramics processing, cannot be treated as sequential. In the design process documented in this thesis, decisions made within each area constrain and redirect the others. The following sections therefore introduce not just background material, but the vocabulary that will reappear throughout the later chapters.

2.1 Pressure Waves and the Wave Equation

At first glance, defining sound may appear trivial, as we are constantly interacting with the sound around us. However, in the field of acoustics, a precise definition is required: *Sound is the propagation of pressure fluctuations through an elastic medium* [3, 4]. In the context of a loudspeaker driver, as depicted in fig. 2.1, when the speaker membrane vibrates, it displaces the air particles immediately in front of it. These particles in turn displace the neighbouring particles, and the disturbance continues propagating outward as a *pressure wave*. These disturbances eventually reach your ear, and your brain then interprets this as sound. These pressure waves abide by the physical equation known as the wave equation:

$$\nabla^2 p = \frac{1}{c^2}\frac{\partial^2 p}{\partial t^2}, \tag{2.1}$$

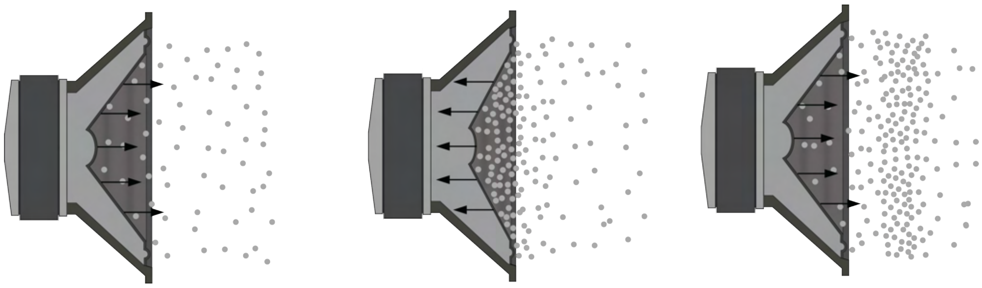

Figure 2.1: Speaker pushing air particles

where c is the speed of sound in the medium and ∇^2 is the Laplacian operator.[1] In one spatial dimension this reduces to

$$\frac{\partial^2 p}{\partial x^2} = \frac{1}{c^2}\frac{\partial^2 p}{\partial t^2}. \tag{2.2}$$

The derivation of the wave equation will not be shown here but can be found in Kinsler et al. [6] *Fundamentals of Acoustics*. The derivation combines the conservation of momentum (Euler equation) with the continuity equation (conservation of mass), assuming small perturbations [4, 6, 7]. Solving this equation for complex geometries can be highly abstract, as such the following sections introduce the *1D mass-spring oscillator* as an analogy to build intuition for concepts such as resonance, frequency response, continuous bodies, and acoustic impedance.

2.2 The Damped, Driven 1D Oscillator

The oscillation of a particle in an elastic medium can be modelled using the *one-dimensional mass-spring oscillator* [6]. To accurately represent a real loudspeaker system, the model consists of a point mass m, stiffness k, damping coefficient C, and a harmonic external driving force $f(t) = F\cos(\omega t)$ [6, 8]. Balancing these forces yields the equation of motion:

$$m\ddot{x} + C\dot{x} + kx = f(t). \tag{2.3}$$

[1]The Laplacian operator acts as a multidimensional equivalent of the second derivative [5].

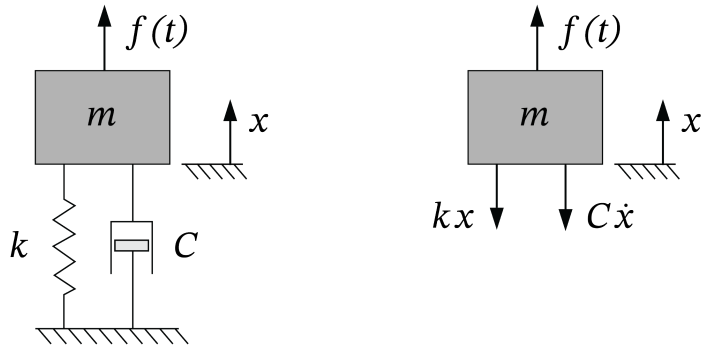

Figure 2.2: Mass-spring system with free body diagram.

As detailed in appendix A, the complete solution consists of a temporary transient response and a persistent steady-state response [7]. As the transient components decay over time due to system damping, the steady-state response, where the system oscillates continuously at the driving frequency, is of primary interest when evaluating audio equipment, as visualized in fig. 2.3 [4].

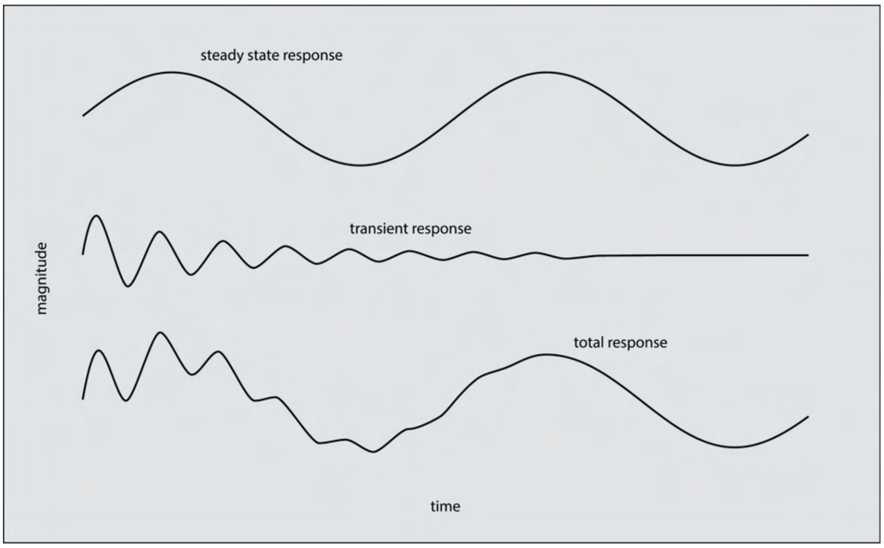

Figure 2.3: Transient and steady-state components of the damped driven oscillator response.

2.3 Resonance and Frequency Response

Every oscillatory system has a *natural frequency* ω_0, defined as the angular frequency at which the system freely oscillates. For the mass-spring system, this is given as

$$\omega_0^2 = \frac{k}{m} \quad [8].$$

However, depending on the level of damping, the damped natural frequency ω_d may differ from the undamped natural frequency. For a lightly damped mass, the damped natural frequency satisfies $\omega_d \approx \omega_0$ [6, 7].

For a harmonically driven system of this nature, the steady-state amplitude depends on the driving frequency ω. This relationship, known as the frequency response, describes how the system responds across a sweep of frequencies, see fig. 2.4.

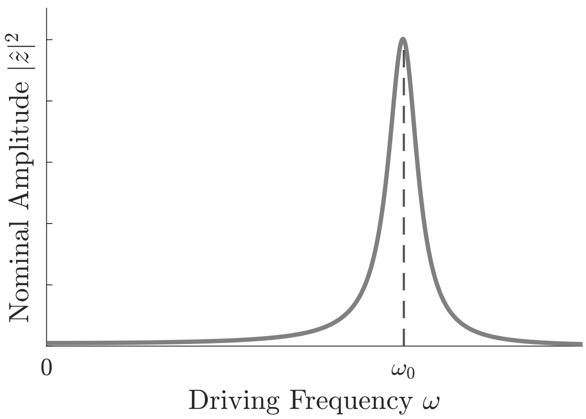

Figure 2.4: Frequency response of the damped driven oscillator.[2]

From fig. 2.4 it can be observed that as the driving frequency ω approaches ω_0, the steady-state amplitude reaches a maximum. This phenomenon is known as resonance and if a system has very low internal damping, this resonance peak becomes exceptionally sharp and violent, which can severely destabilise acoustic performance and introduce structural coloration. Conversely, higher internal damping absorbs this energy, smoothing out the frequency response curve.

[2]The real-valued displacement x is commonly replaced with a complex-valued z, see appendix A.

2.4 Coupled Oscillators and Normal Modes

Real continuous structures are far more complex than single isolated particles. If two discrete mass-spring systems are linked together as depicted in fig. 2.5, the system undergoes *frequency splitting*. Instead of a single natural frequency, the system now exhibits two distinct natural frequencies, each corresponding to a unique *normal mode* shape [7, 9]. In the first mode, both masses vibrate at a specific frequency completely in-phase; in the second mode, they vibrate at a different frequency out-of-phase, see fig. 2.6.

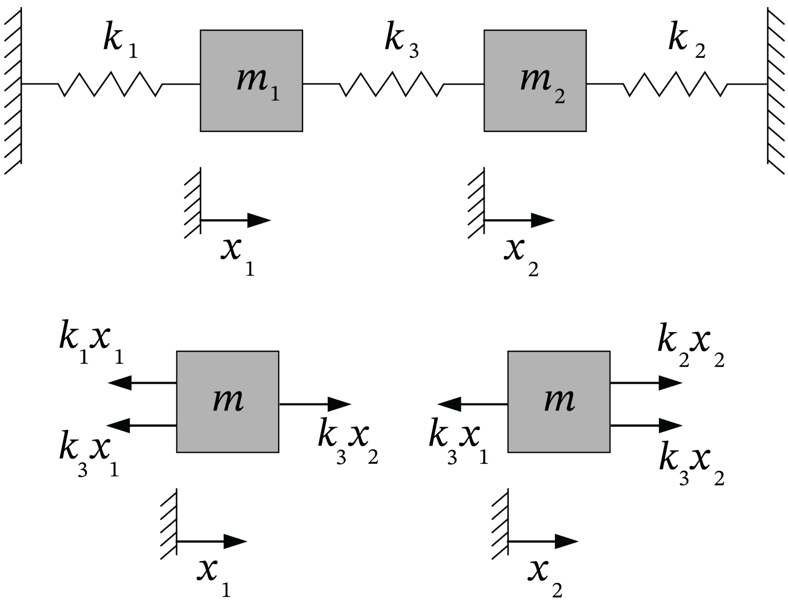

Figure 2.5: Coupled 1D mass-spring oscillator.

A critical takeaway of this behavior is that a system with N degrees of freedom will possess exactly N natural frequencies and N associated mode shapes [7].

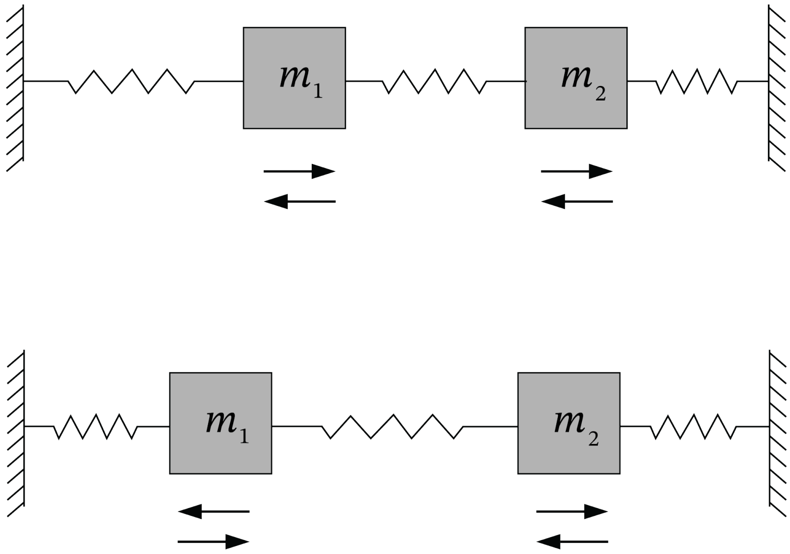

Figure 2.6: Normal modes of the coupled oscillator.

2.5 Continuous Systems and Structural Resonances

Extending this logic to a solid body such as the physical shell of an acoustic horn the structure can be conceptualised as an infinite mesh of these coupled oscillators extending through three-dimensional space, see fig. 2.7. However, in reality the discrete springs are replaced by continuous material elastic constants (Young's modulus E, Poisson's ratio), and the point masses are replaced by mass density ρ [10]. Consequently, a physical horn shell possesses a vast spectrum of structural normal modes. If the high-pressure acoustic field inside the horn excites these structural wall resonances within the audible range, the horn walls will physically vibrate and colored sound waves will radiate into the room, resulting in a resonance peak in the frequency response and driving up Total Harmonic Distortion (THD) as discussed later in section 2.11.

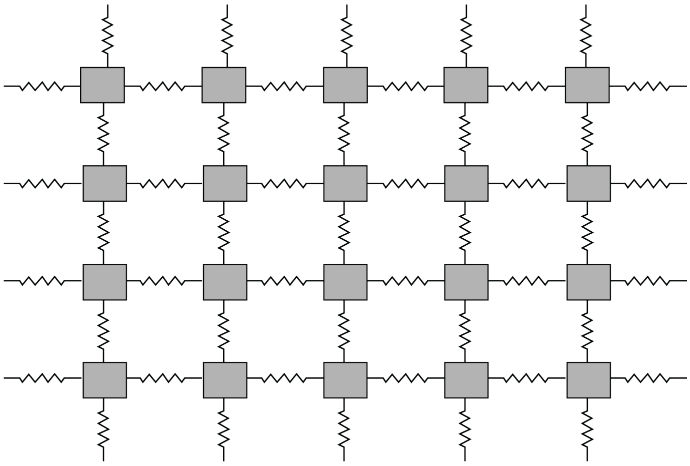

Figure 2.7: Mesh of coupled 1D oscillators.

This continuous framework highlights why material selection is a defining engineering variable. Stoneware ceramics exhibit a Young's modulus of 50–70 GPa, which is dramatically higher than typical 3D-printed PLA plastics at 3–4 GPa [11]. Although ceramics are also denser than PLA, their exceptionally high stiffness-to-density ratio increases the velocity of elastic waves propagating through the horn walls. This structural rigidity drives the system's structural normal modes to significantly higher frequencies compared to an equivalent PLA horn. Whether these resonances fall within or above the operating range of the compression driver, and whether they meaningfully affect the radiated sound, is one of the questions motivating the acoustic evaluation presented later in this thesis.

2.6 Acoustic Impedance and Energy Transfer

To quantify how effectively an acoustic radiator transfers energy into the surrounding air, it is necessary to introduce the concept of impedance. Building on the mechanical framework, the *mechanical impedance* Z_m represents the ratio of the complex driving force to the resulting velocity:

$$Z_m = \frac{F}{\dot{x}} \quad [6, 8]. \tag{2.4}$$

This property characterises how strongly a physical system resists motion when subjected to an external driving force.

To build intuition, this mechanical system can be mapped to a mathematically identical electrical *RLC circuit*, as illustrated in fig. 2.8 [6]. Under this standard engineering analogy, physical mass (m) acts like electrical inductance (L), mechanical damping (C) acts like electrical resistance (R), and structural stiffness (k) acts like inverse capacitance ($1/C$). Just as the resonance of an RLC circuit dictates electrical current flow, this mechanical-electrical equivalence shows that total impedance is split into two parts: a *resistive* component (associated with real energy dissipation or acoustic radiation) and a *reactive* component (associated with temporary energy storage without loss).

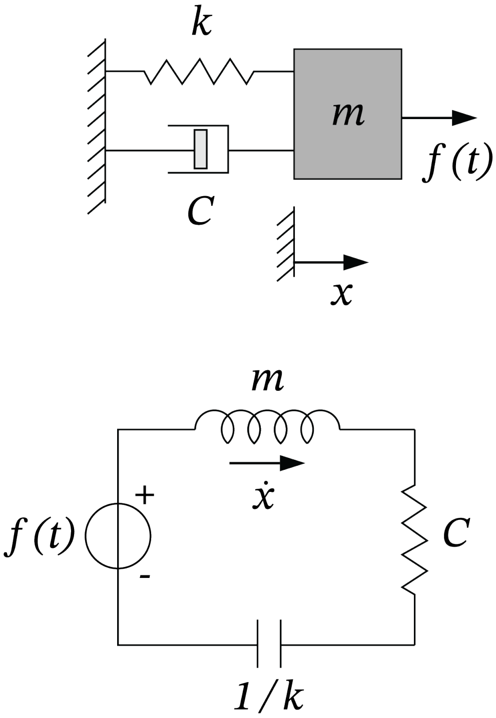

Figure 2.8: Mass-spring and RLC circuit equivalence.

Extending this framework from mechanics to acoustics, the *acoustic impedance* Z_s characterises the behaviour of travelling pressure waves and is defined as the ratio of acoustic pressure to particle velocity:

$$Z_a = \frac{p}{v} \quad [8]. \tag{2.5}$$

When an acoustic source is poorly matched to its surrounding environment, the load becomes predominantly reactive. Energy becomes trapped near the source, oscillating uselessly back and forth in the near field. This mismatch directly describes the inefficiency of a bare loudspeaker diaphragm. The mechanical impedance of a direct-radiating diaphragm is orders of magnitude higher than the fluid load of open air, resulting in exceptionally poor coupling efficiency, particularly at lower frequencies. Understanding this distinction between resistive radiation and reactive energy storage forms the theoretical foundation for horn loading explored in the following sections.

2.7 Horns and Horn Loading

A horn is a waveguide characterized by a continuously increasing cross-sectional area, as illustrated in fig. 2.9. The narrow entrance, termed the *throat*, couples directly to the acoustic transducer, while the wider exit, the *mouth*, radiates into the surrounding environment. Although colloquially described as devices that "amplify" sound, a horn is a passive component that cannot add energy to the system. Instead, it functions as an *acoustic transformer*. It gradually converts the high-pressure, low-particle-velocity environment at the throat into the low-pressure, high-particle-velocity field at the mouth.

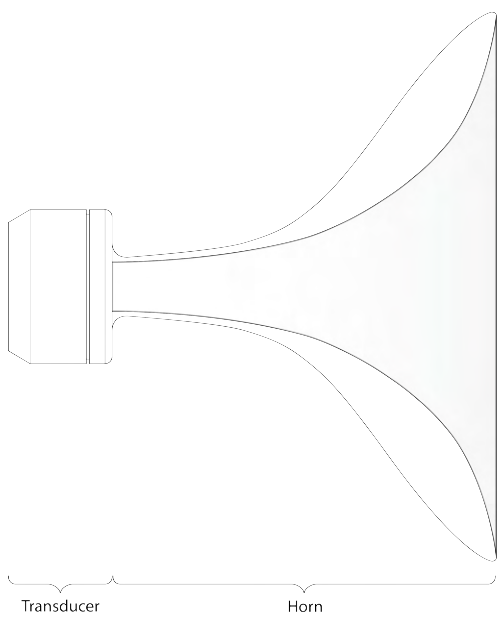

Figure 2.9: Schematic of a horn showing the continuous increase in cross-sectional area from throat to mouth. The gradual taper enables impedance matching from the transducer to free air.

This transformation directly resolves the severe impedance mismatch of direct-radiating transducers highlighted in section 2.6. By providing a controlled, physical boundary for the expanding wavefront, the gradual flare of the horn suppresses internal reflections and dramatically increases the resistive component of the acoustic impedance seen by the diaphragm. Consequently, instead of storing reactive energy in the near field, a significantly larger fraction of the mechanical energy is converted into real radiated acoustic power. This mechanical-to-acoustic coupling process is known as *horn loading*.

Beyond improving radiation efficiency, the structural boundary of the horn walls restricts the unhindered spherical spreading of acoustic waves. By constraining the expansion of the wavefront, the horn inherently concentrates acoustic energy along its central axis, thereby increasing the *directivity* of the transducer [12]. Controlling this directivity is highly advantageous in applications requiring tight coverage patterns and high sensitivity, making it a foundational element in professional cinema systems and high-efficiency loudspeaker designs.

2.8 Cut-off Frequency

A critical consequence of a waveguide's geometry is that efficient acoustic energy transfer is restricted to a certain frequency range. The physical mechanism behind this threshold depends entirely on the profile's expansion rate.

In idealized classical horns, such as an exponential profile, the uniform rate of cross-sectional area expansion establishes a sharp lower frequency limit known as the cut-off frequency (f_c). Below this distinct frequency boundary, the acoustic throat impedance shifts entirely from resistive to reactive, causing internal acoustic energy to build up near the throat rather than radiating effectively out of the horn mouth [13]. However, for many modern horn profiles this acoustic transition occurs gradually over a wider frequency band rather than at a singular cut-off point.

Ultimately, this lower boundary acts as a critical design parameter. To maintain continuous resistive acoustic loading across the driver's entire operating range, the waveguide's physical length, flare profile, and mouth size must be engineered to support frequencies at or below the driver's lowest cutoff.

2.9 Compression Drivers

A *compression driver* is a type of high-frequency transducer commonly used in combination with a horn loudspeaker. Unlike a conventional loudspeaker, where the diaphragm couples directly to free air, a compression driver forces the acoustic energy from the diaphragm through a narrow throat into the horn, as shown in fig. 2.10.

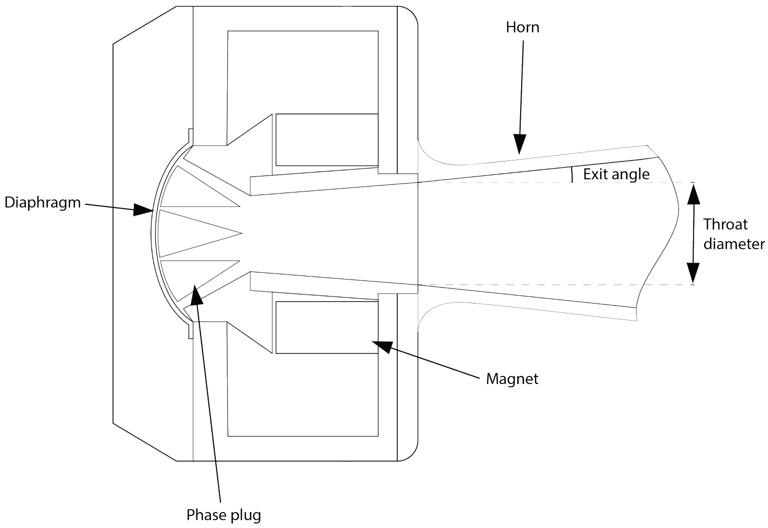

Figure 2.10: Schematic of a compression driver coupled to a horn throat.

This configuration provides two key advantages. First, the restricted throat area acts like a nozzle, concentrating the air pressure at the entrance of the horn. This allows the driver to transfer energy into the air much more effectively than a standard cone speaker, significantly increasing overall acoustic efficiency. Second, the small pocket of air trapped in the compression chamber modifies the mechanical loading on the diaphragm, which helps extend its effective high-frequency response.

Key specifications of compression drivers provided in manufacturer datasheets include:

- **Throat diameter:** The diameter of the driver exit, which must match the horn throat for efficient acoustic coupling.
- **Exit angle:** The angle at the exit of the compression driver, usually given as the half-angle.

- **Recommended crossover frequency:** The lowest frequency at which the driver is intended to operate safely and linearly when paired with a horn. Operating below this frequency may result in increased distortion or diaphragm overload.
- **Nominal impedance:** The rated electrical impedance of the driver (commonly 8 Ω or 16 Ω), used for amplifier matching and crossover design.
- **Power capacity (AES):** The continuous power the driver can withstand under standardised AES testing conditions.
- **Peak power capacity:** The maximum short-term power the driver can tolerate without mechanical or thermal failure.

2.10 Frequency Response in Loudspeaker Evaluation

Loudspeaker performance is primarily evaluated by its frequency response, which is assessed by measuring the *sound pressure level* (SPL) across the audible spectrum in response to a constant-amplitude input signal. These measurements are conducted both on-axis (directly in front of the acoustic source) and off-axis at various angles to fully capture the loudspeaker's *directivity*[3].

According to Toole [14], loudspeaker quality is largely determined by its ability to deliver a neutral, uncoloured acoustic response. This relies on two primary criteria: a flat on-axis frequency response and smooth off-axis directivity. While the on-axis response should ideally be flat when measured in an anechoic environment, a significant portion of the perceived sound in a typical listening room consists of *early reflections*. These are acoustic waves that arrive at the listener shortly after the direct sound after reflecting off nearby room boundaries [8, 15]. Because the spectral content of these early reflections is governed by the loudspeaker's off-axis radiation, the off-axis response must vary smoothly and maintain a similar curve to the on-axis response for perceptually neutral reproduction. Consequently, abrupt irregularities in directivity are perceived as audible resonances, even if the direct on-axis response is perfectly flat [14].

[3] The degree to which an acoustic radiator concentrates sound energy in specific directions.

2.11 Total Harmonic Distortion

Another important measure of loudspeaker performance is the total harmonic distortion (THD). An ideal loudspeaker would respond linearly to its input: a sinusoidal signal at frequency f_1 would produce an output at exactly f_1, scaled in amplitude. Real transducers deviate from this ideal. Nonlinearities are unavoidable and cause the output to contain not only the fundamental frequency but also components at integer multiples, known as *harmonics* [14, 15].

For a sinusoidal excitation at frequency f_1, a nonlinear system produces output components at $f_1, 2f_1, 3f_1, \ldots$ with amplitudes $A_1, A_2, A_3, \ldots$ respectively. THD quantifies the relative magnitude of these harmonic components with respect to the fundamental,

$$\mathrm{THD} = \frac{\sqrt{A_2^2 + A_3^2 + \cdots + A_n^2}}{A_1}, \tag{2.6}$$

and is typically expressed as a percentage [16]. A lower THD indicates a more linear system.

Elevated THD within the operating range of the horn can indicate structural or material resonances within the horn walls themselves, making it a valuable tool for assessing how the mechanical properties of the ceramic material affect acoustic performance.

2.12 Horn Profiles

As discussed in the previous sections, the geometry of a horn determines both its impedance-matching behaviour and its directivity. This section outlines the mathematical foundations behind horn profiles designed to control wavefront propagation, drawing heavily on Bjørn Kolbrek's *Horn Theory: An Introduction* [13].

A central factor in the choice of geometry is the assumed wavefront shape inside the waveguide. Classical one-dimensional horn models operate under the assumption that pressure is perfectly uniform across the cross-section, which describes a plane wave. In physical horns, however, wavefronts are inherently curved. Profiles that mathematically account for this curvature produce an environment that minimizes internal reflections and matches real physical behavior much more accurately. The *Kugelwellen* (spherical-wave) horn and the *oblate spheroidal* horn are two such profiles, each resolving the plane-wave limitation through distinct geometric assumptions.

2.12.1 Kugelwellen Profile

The Kugelwellen horn (derived from the German for *spherical waves*) was developed by Klangfilm, the motion picture division of Siemens, in the late 1940s [1]. It is based on the assumption that the wavefronts inside a horn expand as spherical surfaces with a constant radius r_0 [13]. This physically reflects the fact that a compression driver throat behaves more like a localized radiating sphere than a flat, infinite piston. In addition to this geometric assumption, the total wavefront area expands exponentially along the longitudinal axis of the horn.

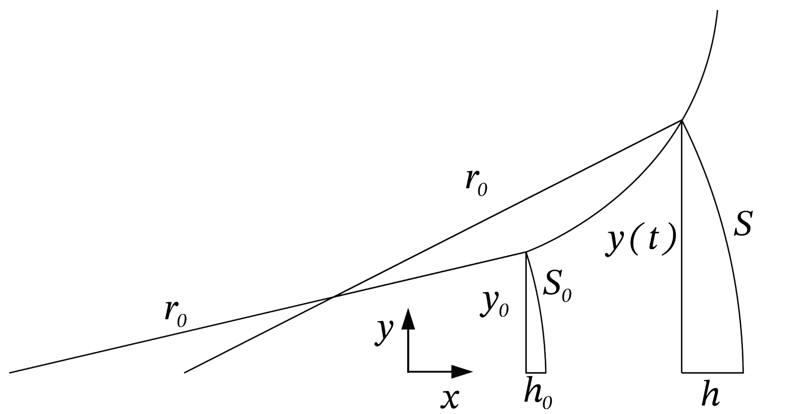

Figure 2.11: Schematic of the Kugelwellen defining parameters.

At any position along the horn, the expanding spherical wavefront is modeled as a *spherical cap*. This is the surface area obtained by cutting a sphere with a transverse plane, as illustrated in fig. 2.12. The geometry of this cap is defined by its height h, measured from the base of the cap to the peak of the spherical surface.

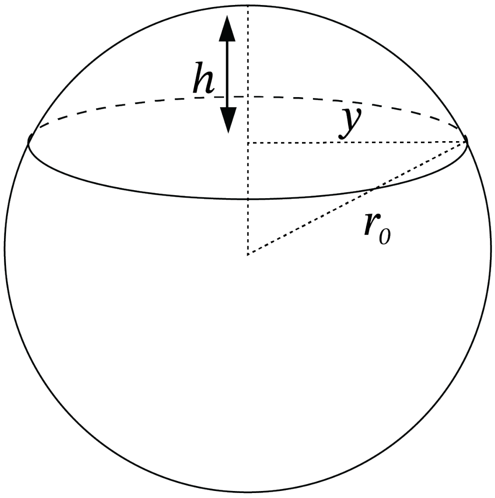

Figure 2.12: Spherical cap geometry.

The constant wavefront radius of the Kugelwellen horn is described as:

$$r_0 = \frac{c}{\pi f_c}, \tag{2.7}$$

where c is the speed of sound and f_c is the cut-off frequency. At the throat entrance where the physical horn radius is y_0, the corresponding spherical cap height is:

$$h_0 = r_0 - \sqrt{r_0^2 - y_0^2}, \tag{2.8}$$

and the wavefront surface area follows the mathematical spherical cap relation $S = 2\pi r_0 h$. For this area to expand exponentially, the cap height h must also increase exponentially, allowing the height to be written parametrically as:

$$h(t) = h_0 \, e^{m\xi t}, \qquad t \in [0, 1], \tag{2.9}$$

where $m = 4\pi f_c / c$ represents the flare constant and ξ serves as a geometric truncation parameter.

The radial coordinate $y(t)$ and axial coordinate $x(t)$ of the physical horn wall follow directly from this spherical geometry:

$$y(t) = \sqrt{2r_0 h(t) - h(t)^2}, \qquad x(t) = \xi t - h(t) + h_0. \tag{2.10}$$

Together, eqs. (2.9) and (2.10) define the Kugelwellen horn profile parametrically, originating at the throat at $t = 0$ and terminating at the mouth at $t = 1$. A unique structural property of the pure Kugelwellen profile is that it folds back on itself, as depicted in fig. 2.13. This geometric roll-back ensures that the acoustic wavefront is gently released into free space, significantly reducing edge diffraction and boundary reflections at the mouth [13].

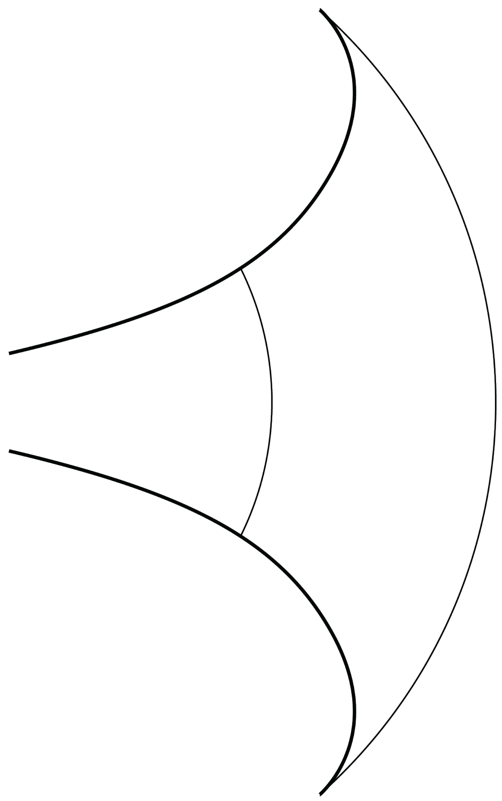

Figure 2.13: Foldback profile of the Kugelwellen horn.

The resulting profile is governed by three free parameters: f_c, y_0, and ξ. In physical applications, f_c is closely constrained by the compression driver, as the initial wall angle at $t = 0$ must match the exit angle of the source to avoid a curvature discontinuity. This boundary condition effectively fixes the wavefront radius and flare constant. The remaining parameters control the start and endpoints of the profile. The throat radius y_0 establishes the entry point along the curve (fig. 2.14a), while the truncation parameter ξ sets the endpoint along the profile (fig. 2.14b).

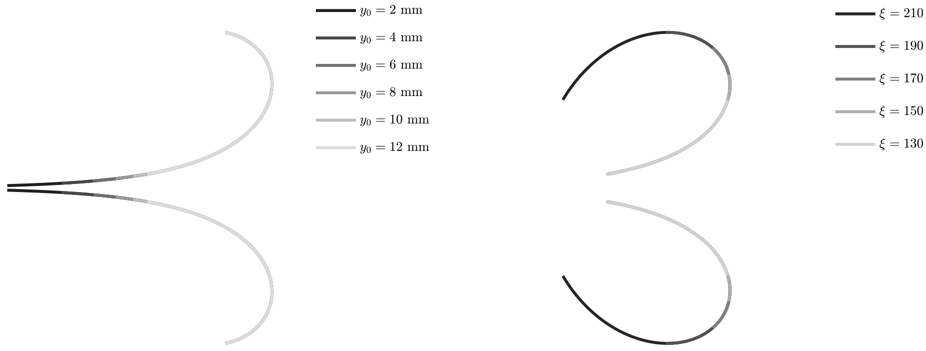

(a) Varying y_0 with fixed ξ: the throat radius shifts the entry point along the curve.

(b) Varying ξ with fixed y_0: the truncation parameter sets the end point of the curve.

Figure 2.14: Effect of the free parameters on the Kugelwellen geometry.

2.12.2 Oblate Spheroid Profile

The oblate spheroid (OS) horn, developed by Geddes [17, 18] based on foundational work by Freehafer [19], offers an alternative wavefront assumption. Similar to the Kugelwellen geometry, the OS profile accounts for the finite throat area of real compression drivers. Rather than assuming flat plane waves, it treats the expanding wavefronts as *oblate spheroids*. These are three-dimensional, flattened sphere-like surfaces [13, 17].

The primary acoustic advantage of the OS profile is that the directivity is dictated explicitly by a single design parameter: the coverage half-angle α. Consequently, the designer can precisely set the waveguide's dispersion pattern to maintain constant directivity across the operating frequency, satisfying the acoustic requirements outlined in section 2.10.

2.12.2.1 Profile Geometry

The OS wall radius as a function of axial distance z is expressed mathematically as:

$$r_{\mathrm{OS}}(z) = \sqrt{r_0^2 + 2r_0 z \tan(\alpha_0) + z^2 \tan^2(\alpha)}, \tag{2.11}$$

where r_0 is the entry throat radius (note that this is not the same r_0 as for the Kugelwellen) and α_0 is the throat half-angle which can easily be set to match the exit angle of the compression driver [20]. Geometrically, this expression describes a hyperbola in the (z, r) coordinate plane.

Because a pure mathematical OS profile represents an infinitely long curve, physical implementation requires the waveguide to be truncated at a finite length L and transitioned smoothly into a termination profile. As illustrated in fig. 2.15, two standard termination geometries are: a *superelliptical* profile, which curves the wall to a 90° mouth to sit flush within a flat baffle, and a *clothoid* profile, which rolls the wall back gradually past 90° making it optimal for external horns [20].

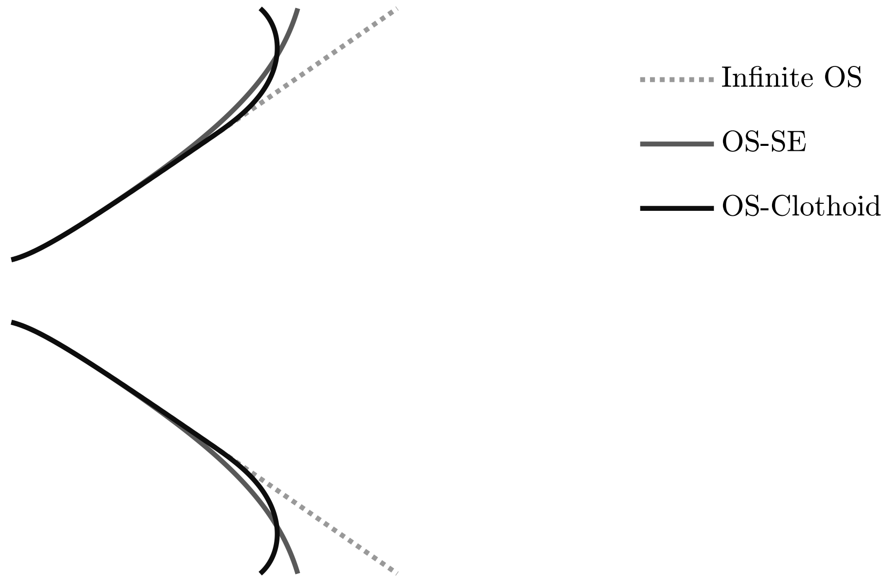

Figure 2.15: OS profile termination comparison showing superelliptical and clothoid variations.

2.12.2.2 Clothoid Termination

A clothoid (alternatively termed an Euler or Cornu spiral) is defined as a curve whose physical curvature increases linearly as a function of its arc length. This property makes it an ideal geometric bridge for smoothly mating the OS hyperbola to the surrounding air. The wall angle increases continuously until the edge rolls back to the final exit target. This roll-back rate is dictated by a scale parameter A, where a larger value yields a longer, more gradual geometric sweep.

To achieve an optimal acoustic profile, the boundary interface between the OS hyperbola and the clothoid curve requires G^2 curvature continuity. Ensuring that both the first derivative (slope) and second derivative (curvature) match exactly at the intersection eliminates physical kinks and sudden steps in curvature.

2.12.2.3 Parameters and Physical Interpretation

The final geometry of the OS waveguide with a clothoid termination depends on three parameters: r_0, α_0, and α. Because the chosen driver fixes the throat radius r_0 and initial angle α_0, the coverage angle α is the only free variable used to control the waveguide's dispersion (fig. 2.16a). Additionally, the total horn length L and the clothoid scale factor A determine the mouth's dimensions, controlling how smoothly the waveguide flares out into the surrounding room (fig. 2.16b).

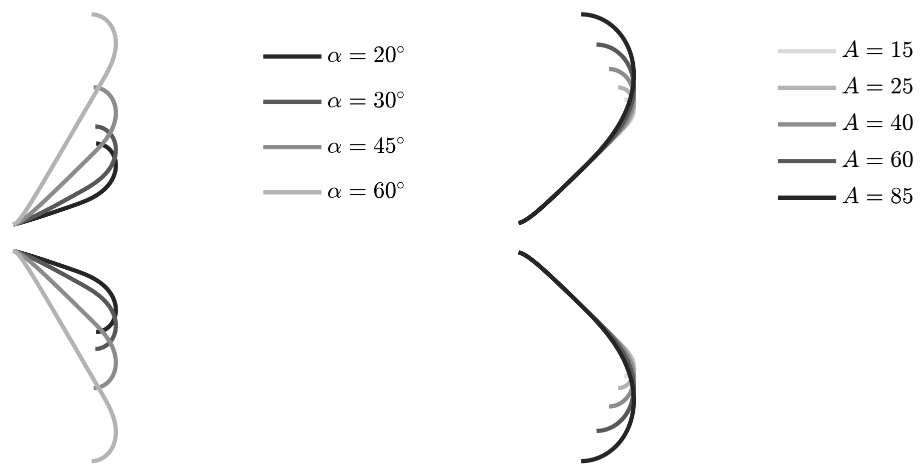

(a) Effect of coverage angle α on the OS profile.

(b) Effect of scale parameter A on the termination curve.

Figure 2.16: Parametric sensitivity analysis of the free variables altering the OS geometry.

2.12.3 Manufacturing Considerations

While these horn profiles are derived primarily from acoustic considerations, it is important to note that their physical realisation is also influenced by manufacturing constraints and material behaviour. In forming processes, geometric features such as wall curvature, transitions, and termination geometry cannot be detached from the manufacturability. As a result, the implementation of mathematically defined horn profiles involves considerations extending beyond acoustic optimisation alone.

2.13 Ceramics and the Ceramic Process

In materials science, ceramics are defined as inorganic, non-metallic compounds composed of metallic and non-metallic elements [11]. This is a broad definition, covering a wide range of materials with different compositions and microstructures. Despite this, ceramics share several characteristic properties that arise from their predominantly ionic and covalent bonding: ceramics are typically stiff, brittle, temperature resistant, chemically stable, and insulating [21].

From an acoustics perspective, the most relevant of these is their high stiffness, i.e. a high Young's modulus. As discussed in section 2.5, this has a direct influence on modal behaviour.

2.13.1 Clay Bodies

This research focuses on clay-based ceramics. Clay is not a single material but a family of naturally occurring mixtures consisting primarily of clay minerals such as kaolinite, along with materials such as quartz and mica [21]. A *clay body* refers to a specific composition of these components.

Clay bodies are often grouped into three broad categories:

- **Earthenware:** fired at relatively low temperatures, remains porous and is generally softer and more workable.
- **Stoneware:** fired at higher temperatures, becomes denser and stronger, with reduced porosity.
- **Porcelain:** fired at the highest temperatures, highly vitrified, very dense and stiff, often with a fine microstructure.

In practice, however, these categories are not sharply defined. Even clay bodies sold under the same name, by the same manufacturer, can vary in composition, and therefore in behaviour [22]. For this reason, working with clay often involves a degree of experimentation, and material properties are frequently determined empirically.

Throughout this report, the term *ceramics* will be used when referring generally to clay-based materials, unless a more specific distinction is required.

2.13.2 The Ceramic Process

The ceramic process can be divided into three stages: forming, drying, and firing. Each stage plays an important role in determining the final properties of the material.

2.13.2.1 Forming

Ceramic forming methods include hand building, wheel throwing, and slip casting. Hand building and throwing fall under *hydroplastic forming*, where the clay contains enough water to be soft and workable [11]. At this stage, the clay is known as a *green body*, and it is the water content that allows it to hold together while being shaped without cracking.

Slip casting differs in that it uses a liquid clay suspension (slip). This method is discussed in more detail in section 2.14.

2.13.2.2 Drying

After forming, the green body is dried to remove water. This process can be deceptively challenging, as non-uniform drying leads to non-uniform shrinkage and internal stresses, which can cause defects such as cracking or warping [11].

Two commonly referenced stages of drying are:

- **Leather hard:** partially dried, firm but still workable; this is often the stage where trimming and refining the form takes place.
- **Bone dry:** fully dried, no remaining plasticity and very fragile.

The bone dry stage is typically the weakest point in the process, as the material has lost its ductility but the clay has to reach this stage before it can go on to be fired.

2.13.2.3 Firing

Firing transforms the dried clay into a strong ceramic. The initial firing stage, known as *bisque firing*, is conducted at relatively low temperatures (900–1000C) to increase strength while maintaining porosity.

Subsequently, the ceramic is commonly glazed, which involves applying a thin coating to the surface. Glazes can vary widely in composition and appearance, allowing for a large range of surface finishes, colours, and textures as illustrated by the glaze samples in fig. 2.17. This is one of the key areas where the material offers significant artistic expression, which is why many ceramists are highly selective about their glazes. In addition to aesthetics, glazes can also affect surface properties such as smoothness and permeability.

Figure 2.17: Glaze samples.

After glazing the ceramic then undergoes a *glaze firing*, typically performed at higher temperatures, during which the material undergoes significant *vitrification* that determines its final properties [11].

2.13.3 Vitrification

A key process during firing is *vitrification*. As the temperature increases, some of the particles within the clay begin to melt and form a liquid phase. This liquid flows into the pores between particles and, upon cooling, solidifies into a glassy matrix. The final structure typically consists of a mixture of this glassy phase, remaining solid particles, and some residual porosity.

The degree of vitrification strongly influences the material properties. Increased vitrification leads to higher density, strength, and durability [11].

2.13.4 Shrinkage

Shrinkage occurs during both drying and firing as water is removed and the material densifies. The extent of shrinkage depends on the clay composition, water content, and firing temperature.

In practice, shrinkage is often determined empirically by making test pieces and measuring the change in dimensions after firing. It is often assumed that clay shrinkage is isotropic for simplicity, though this is not strictly accurate [23].

2.14 Slip Casting

A slip is a suspension of clay in water. In slip casting, this liquid clay is poured into a porous plaster mould. The plaster absorbs water from the slip, causing a solid layer of clay to form along the mould wall. The thickness of this layer increases with time, allowing some control over the final wall thickness.

As the cast piece dries, it shrinks slightly and eventually releases from the mould surface, at which point the mould can be opened and the piece removed. Details regarding plaster preparation are provided in appendix B.

2.14.1 Variations of Slipcasting

Slip casting can be divided into two main variations: *drain casting* and *solid casting*.

Drain casting involves allowing the slip to form a layer along the mould wall for a set period of time, after which the excess liquid slip is poured out [11]. This results in a shell-like object with uniform wall thickness, as illustrated in fig. 2.18.

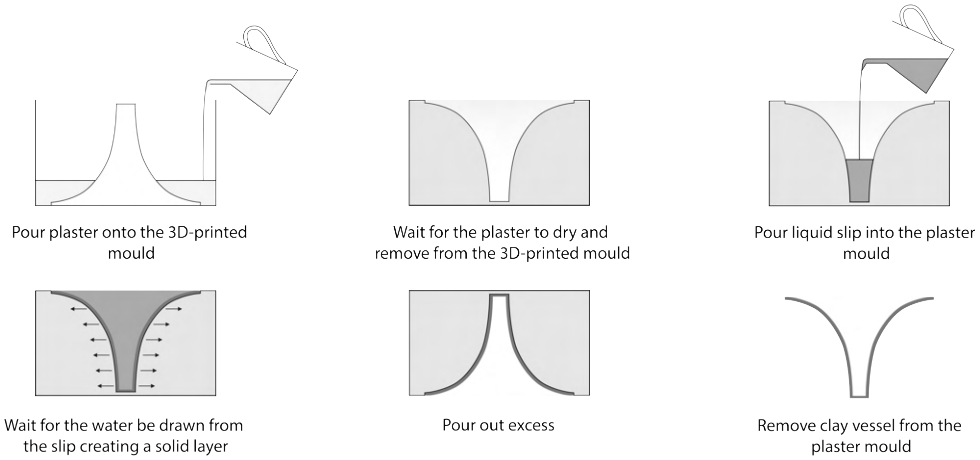

Figure 2.18: Drain casting process with 3D printed mould positives.

In contrast, solid casting involves leaving the slip in the mould until the entire volume solidifies [11]. For geometries such as horn structures, this approach typically requires a multi-part mould with an internal core, as shown in fig. 2.19.

Figure 2.19: Solid casting process using a multi-part mould with an internal core.

2.15 Designing for Solid Casting

Designing for slip casting requires careful consideration, as the manufacturing process imposes significant constraints on the geometry. Solid casting, in particular, allows for greater variation in wall thickness, but introduces additional challenges that must be accounted for during the design stage.

2.15.1 Parting Line Placement

Parting line placement is a fundamental step in mould design, as it determines whether a geometry can be cast at all. The mould must be separable, meaning that no *undercuts* can be present that would prevent the mould sections from being removed.

In addition, the geometry of the plaster mould itself must be considered. Plaster is brittle, and thin sections or sharp corners are prone to breaking during handling.

Each parting line also results in a seam (flash) on the final ceramic piece. These seams should therefore be placed in locations where they are either easy to clean up or intentionally integrated into the design.

2.15.2 Air Pockets and Pour Direction

The direction in which the mould is filled has a direct impact on the formation of air pockets. During solid casting, the mould is filled completely, and air must be able to escape as the slip fills the volume. This typically requires the inclusion of air holes in the mould.

Poorly considered geometry can trap air, leading to defects in the final piece. As such, the design should aim to minimise enclosed volumes and allow for smooth filling of the mould. The location of the pour hole is also important, as it will leave a mark that must be removed or incorporated into the final design.

2.15.3 Wall Thickness

Although solid casting allows for variable wall thickness, there are practical limits. Thick sections significantly increase drying time and make it difficult to ensure that the piece is fully dry before firing.

In addition, the outer surface dries and shrinks faster than the interior, leading to non-uniform shrinkage and an increased risk of cracking. These effects become more pronounced as thickness increases.

It is also important to consider thickness variation along the flow direction of the slip. If a thinner section is encountered early in the filling process, it may solidify quickly and restrict further flow, preventing slip from reaching deeper regions of the mould.

2.15.4 Draft Angles and Demoulding

Although the clay shrinks slightly during drying, draft angles are still sometimes necessary to ensure that the piece can be removed from the mould without damage. This is particularly important when using moulds with internal cores, as is common in solid casting. In these cases, shrinkage causes the clay to grip the core more tightly, increasing the risk of cracking during removal. Adequate draft angles help mitigate this issue.

2.15.5 Manufacturing Implications

Taken together, these constraints illustrate how manufacturing considerations can directly influence the geometric design of cast ceramic components. In applications involving acoustically defined surfaces, such interactions become particularly significant, as small geometric deviations may affect both manufacturability and acoustic performance.

2.16 Casting with 3D Prints

The increasing availability of 3D printing has introduced new possibilities in ceramic mould making. In this workflow, a 3D printed object is used as a positive form, around which a plaster mould is created, taking the role of the *pattern* in traditional metal casting. The 3D print acts as the positive, the plaster mould as the negative, and the ceramic part as the final positive, see fig. 2.18.

This approach allows for the fabrication of geometries that would be difficult to produce using traditional forming methods alone. It also enables a high degree of control over the final shape, making it particularly useful when trying to realise a form that follows a mathematical curve.

3 Methodology

This project combines two complementary methodological strands: an iterative design and fabrication process used to develop ceramic horn prototypes, and acoustic measurements used to evaluate their performance. Together, these strands address the research questions concerning both the feasibility of ceramic horn manufacturing and the acoustic consequences of material choice.

3.1 Research Through Design

The project was not initially conceived as a research through design study. The primary objective was to investigate the feasibility and acoustic performance of ceramic loudspeaker horns. However, answering these questions required the development of horn geometries, mould systems, and manufacturing methods. Consequently, knowledge was generated not only through analysis and measurement, but also through the design and fabrication of physical artefacts.

This perspective aligns with Frayling's concept of research through design, in which practical experimentation functions as a mode of inquiry alongside theoretical investigation [24]. The design process therefore served both as a means of producing prototypes for acoustic evaluation and as a method for investigating the practical constraints of ceramic horn manufacturing, with sketches, CAD models, and mould designs used to assess the feasibility of different design approaches prior to concept realisation.

This approach also shares similarities with the action-oriented form of research described by Frayling, where a practical experiment is documented throughout its development and later contextualised through written reflection [24]. In this project, the logbook presented in appendix C.2 fulfils this role by documenting the sequence of decisions, failures, observations, and revisions that shaped the development process.

3.2 Design and Fabrication Process

The development of the horn prototypes and their associated mould systems formed the practical component of the investigation. The prototypes were developed to a level sufficient to evaluate the feasibility of the manufacturing approach and to conduct the acoustic measurements required to address the research questions. This is consistent with the role of prototypes in constructive design research as described by Koskinen et al. [25]. The objective was therefore not to produce production-ready components, but to realise prototypes capable of supporting both the manufacturing investigation and the comparative acoustic evaluation.

The work is presented using the concept development, detailed design, and concept realisation phases from Ulrich and Eppinger's framework, as introduced in section 1.5 [2]. These phases provide a reporting structure rather than a process model, in practice the work was much more non-linear, with manufacturing outcomes frequently prompting revisions to earlier design decisions.

3.3 Acoustic Evaluation

The completed horn prototypes were evaluated through a comparative experiment designed to isolate the influence of horn material on measurable acoustic behaviour. For each horn geometry developed in the design process, a ceramic prototype and a geometrically equivalent 3D-printed PLA reference horn were measured under identical conditions, allowing direct material comparisons within each geometry. A full account of the experimental setup and measurement procedure is provided in section 7.4.

3.4 Relationship Between the Two Strands

Although the design and fabrication process and the acoustic evaluation are methodologically distinct, they are not independent. The fabrication process determined what prototypes were available for acoustic testing, and the design decisions made throughout such as the choice of horn geometry, clay body, wall thickness, and surface finish which all directly determine what the acoustic measurements can and cannot reveal. Conversely, the acoustic evaluation provided the empirical basis against which the fabrication outcomes could be assessed. The manufacturing strand documents how the horns were made and what that process requires; the comparative experiment investigates whether the material choices involved in that process produce measurable acoustic consequences. Together, they address the three research questions from complementary directions.

4 Concept Development

This chapter documents the early stages of the project, during which design ideas were explored and iterated upon. The process was often non-linear, with multiple ideas being investigated in parallel.

A central aspect of this phase was the close relationship between geometry and manufacturing. Rather than treating design and production as separate stages, the manufacturability of each concept was considered from the outset. As a result, the development of horn geometries and moulding strategies occurred simultaneously.

4.1 Project Framing

The project began with discussions with Tsvetan at the Arda Audio workshop, which helped establish a connection with his vision and broader design language.

Rather than defining a rigid plan from the outset, it felt more valuable to approach the project as a dynamic process. A calendar was used to organise the work, becoming a living document that was continuously updated as new insights emerged, see appendix C.1.

This approach was particularly important given the experimental nature of the project, where multiple processes were often carried out in parallel. As a result, the structure of the project evolved alongside the design itself.

4.2 Initial Design Constraints

Following the initial discussions at the workshop, several constraints were defined to guide the concept development process. The project was confined to ceramic horn manufacturing using slip casting, both due to the author's prior experience with ceramics and because the process aligned well with Arda Audio's existing use of digital fabrication tools.

The investigation focused specifically on horns for high-frequency compression drivers. These horns are central to Arda Audio's product range and are well suited to slip casting due to their relatively compact geometry.

From the outset, manufacturability became a primary design parameter. Shrinkage, demoulding, parting lines, and mould complexity were therefore considered simultaneously with the acoustic geometry during concept development.

4.3 Early Exploration and Iteration

A significant portion of the early phase was devoted to sketching and concept exploration. This section spanned several months prior to the official start of the project, reflecting the more iterative and exploratory development processes often found in small studios. During this period, sketches were produced to investigate both horn geometries and corresponding mould designs.

Early discussions with Uta Koloczek, particularly regarding porcelain casting, helped frame the initial exploration of mould design. These discussions emphasised the importance of considering the casting process from the outset. The focus was not on specifically defined horn profiles, but rather on understanding how different geometries could be manufactured. The rough sketches explored relationships between form, parting lines, and casting feasibility see fig. 4.1.

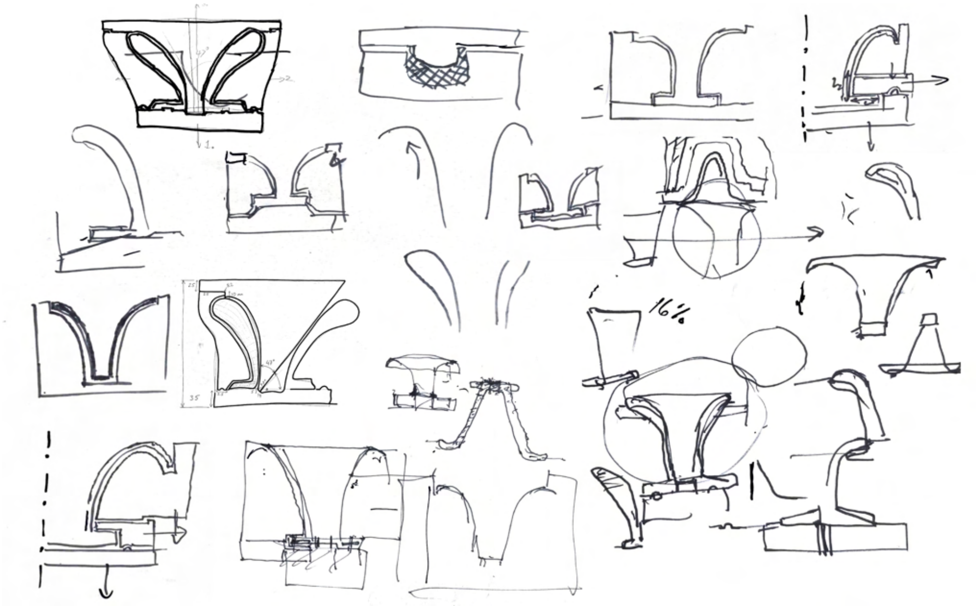

Figure 4.1: A selection of early sketches exploring horn geometries and mould parting strategies.

4.4 Increasing Mould Complexity

An important shift occurred during the early stages of the project. Initially, efforts were made to simplify the mould design, for example by separating the horn geometry from its mounting interface, see fig. 4.2.

However, this approach was later abandoned in favour of integrating the mounting geometry directly into the mould. Although this resulted in more complex multi-part mould assemblies, it simplified the casting workflow itself by reducing the number of post-processing and assembly steps required after casting, see fig. 4.3.

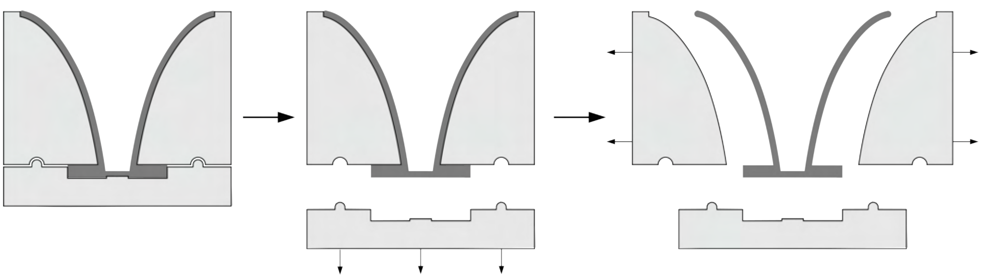

Figure 4.3: Demoulding process for a mould with integrated mounting interface.

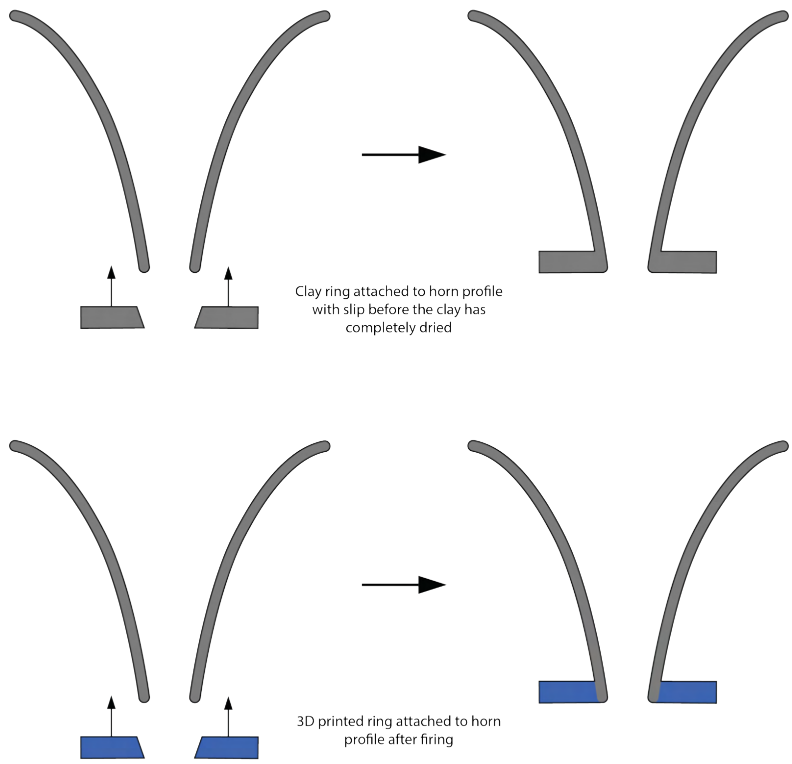

Figure 4.2: Early concepts separating the horn geometry from the mounting interface.

This in turn led to a change in perspective, where the mould and the manufacturing process became as important as the final horn geometry. In this sense, the project evolved from focusing on a single object to developing a system for producing that object. Rather than designing only the horn itself, the work increasingly focused on designing a manufacturing process that minimised post-processing and assembly steps. In this context, Arda Audio effectively became a user of the production workflow developed throughout the project.

4.5 Exploration of Horn Profiles

Several horn geometries were explored in depth during the concept phase, including tractrix and Kugelwellen profiles. These were initially selected due to their relatively simple mathematical definitions and similar overall proportions.

However, the different geometries quickly revealed very different manufacturing challenges. Horns that fold back on themselves, such as the Kugelwellen profile, required moulds with increasingly complex parting strategies, see fig. 4.4. In some cases, demoulding would likely require mould sections to slide relative to one another, increasing the risk of damaging the green body. In addition, the thin overhanging mouth of the horn, would be prone to warping or collapse during drying and firing.

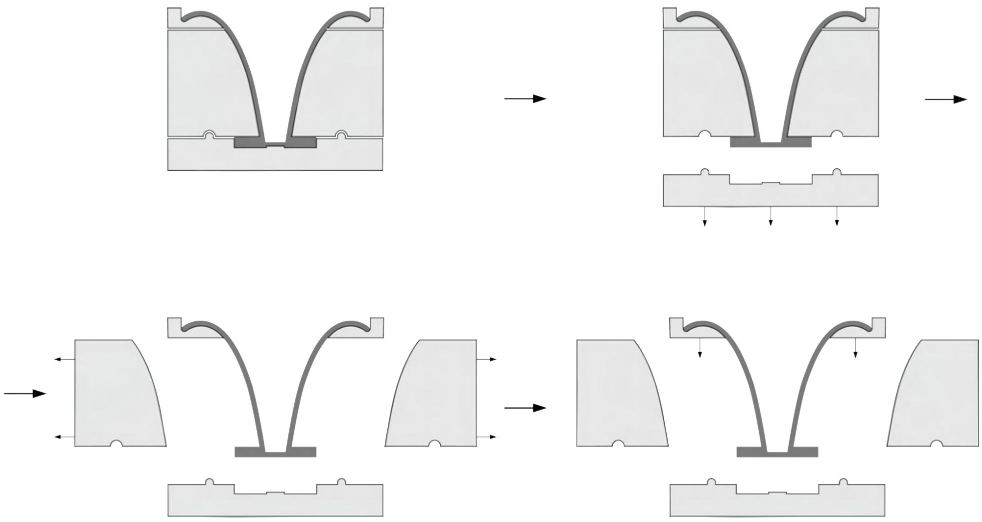

Figure 4.4: Demoulding process for a drain-cast Kugelwellen horn profile.

4.6 Development of Casting Strategies

Initial concepts focused on traditional drain casting, however, with this approach it would be difficult to control the internal geometry of the horn, particularly at the throat where the exit angle of the compression driver is critical. The drain cast horns would have to be drilled during post processing to create the central hole of the horn. This not only complicated compensation for the driver exit angle, but also introduced additional post-processing steps that conflicted with the aim of developing an efficient manufacturing workflow.

To address this, alternative approaches were explored, including the use of internal cores to define the inner horn geometry. Initially a concept with a 3D printed core was conceived as depicted in fig. 4.5.

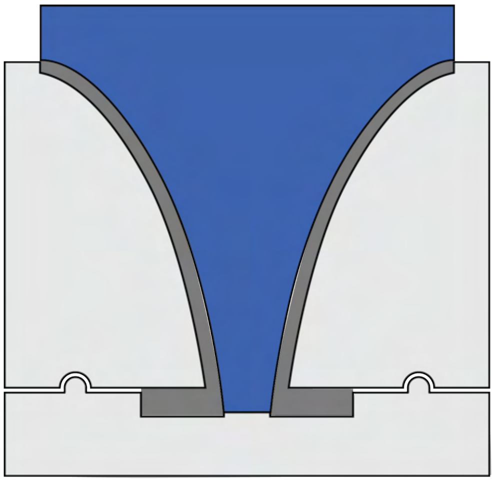

Figure 4.5: Idea for a mould with a 3D printed inner core.

However, discussions with Olof Jansson provided insight into the feasibility of solid casting. While solid casting introduces additional challenges, such as shrinkage around internal cores, it also enables a higher degree of control over the final geometry.

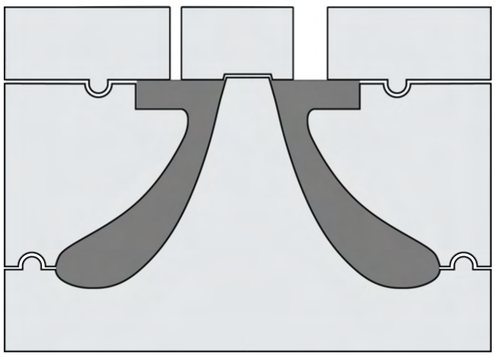

Figure 4.6: Solid cast Kugelwellen horn concept.

4.7 Initial Experimentation Combining 3D Printing and Mould Making

As the concepts increased in complexity, it became clear that the mould-making process would be crucial in determining the success of the project. Initial experiments combining 3D printing and plaster casting were conducted in discussions with Estet Studio to better understand this workflow.

It was assumed that the plaster could be easily removed if sufficient draft angles were included. In practice, the plaster became stuck within the print and had to be forcibly removed, damaging both the 3D prints and the plaster moulds, see fig. 4.7.

Figure 4.7: Initial failed attempt at casting plaster into a 3D-printed form.

This failure provided an important insight that demoulding must be explicitly designed for when combining 3D printing with plaster moulds.

4.8 Design Direction and Selected Horn Profiles

Further discussions with Tsvetan at Arda Audio revealed that many of his horns are based on the oblate spheroid (OS) profile. Combined with the earlier exploration of mould concepts and casting methods, this helped establish a clearer design direction for the project. In particular, it suggested that combining solid casting with more geometrically complex horn profiles could provide practical relevance. It also presented a particularly relevant experimental direction, as solid casting remains relatively uncommon in the production of ceramic horns and therefore introduced a less established set of manufacturing challenges.

The Kugelwellen and oblate spheroid profiles were therefore selected for further development. Both geometries presented different challenges while remaining compatible with the solid casting approach explored during concept development. Using two distinct horn profiles also made it possible to compare how different geometries interact with the same material and manufacturing workflow.

The following chapter focuses on the detailed design and parametrisation of the selected horn geometries and their corresponding mould systems.

4.9 Reflection on the Concept Development Phase

The most significant realisation of this phase was the extent to which manufacturing constraints shaped design decisions from the outset. While this was an explicit goal of the project, the degree to which mould feasibility came to dominate the concept development process was greater than anticipated. This is particularly relevant in the context of small studios such as Arda Audio, where the processes of designing and making are often more closely intertwined than in larger industrial production environments.

However, this strong focus on manufacturability also meant that the formal and aesthetic qualities of the horn geometries received comparatively little attention during this phase, with many decisions regarding outer form being deferred to the CAD stage.

The early sketching phase would likely have benefited from a parallel exploration focused specifically on the visual character of the horns, independent of mould strategy. Earlier investigation of outer form through rough physical models may have informed more considered aesthetic decisions before the geometries were committed to CAD.

5 Detailed Design

This chapter describes the process of developing the chosen horn profiles into manufacturable CAD models and mould designs. The work focused on adapting the chosen geometries to the constraints imposed by ceramic casting while maintaining a visual language consistent with existing Arda Audio horn designs.

It was at this stage of the project that the relationship between geometry and manufacturing constraints became increasingly concrete. Considering how the ceramic horns would be manufactured required continuous negotiation between mould feasibility, material behaviour, and design expression. As a result, the CAD process became a means of reconciling these competing requirements within a manufacturable form.

5.1 Compression Driver Selection and Specifications

The overall dimensions and operating range of the horns were determined by the selected compression driver to which they were to be coupled. Following discussions with Tsvetan, the *BMS 4550* compression driver was selected. This is a professional-grade 1-inch high-frequency compression driver widely used in studio monitors, Hi-Fi systems, and sound reinforcement applications. The driver combines high sensitivity with a relatively low recommended crossover frequency of 800 Hz, making it possible to evaluate the performance of ceramic horns over a broad frequency range while also ensuring that the developed horn prototypes remain relevant to Arda Audio's existing product direction.

A selection of relevant specifications from the BMS 4550 datasheet are provided in table 5.1.

A 2D CAD drawing of the compression driver is also provided in appendix D.

Table 5.1: BMS 4550 specifications [26].

Throat Diameter	1”
Exit angle	14°†
Recommended crossover frequency	800 Hz
Nominal impedance	8 or 16 Ω
Power capacity (AES)	80 W
Peak power	450 W

† Not specified in BMS data sheet, but provided by third-party measurements [27].

5.2 Kugelwellen Parameters

The design of the Kugelwellen horn profile began with the geometric constraints imposed by the compression driver. The driver specifies a throat diameter of one inch ($y_0 = 12.7$ mm) and an exit half-angle of 14°. These values define the boundary conditions from which the horn geometry is derived.

The standard formulation of the Kugelwellen profile does not explicitly account for the exit angle of the driver. However, this was incorporated by evaluating the derivative $\frac{dy}{dx}$ of the profile at the throat $y = y_0$, using the parametric expression given in eq. (2.10).

$$\left.\frac{dy}{dx}\right|_{y=y_0} = \frac{m h_0 (r_0 - h_0)}{y_0 (1 - m h_0)} = \tan\theta_0, \tag{5.1}$$

where θ is the wall half-angle depicted in fig. 5.1.

As $r_0 = c/(\pi f_c)$, the relationship above depends only on the geometric parameter f_c it could be numerically solved in MATLAB yielding (see appendix E.1):

$$f_c = 1043 \text{ Hz}. \tag{5.2}$$

It is worth noting that, unlike exponential horns, where f_c corresponds to a strict acoustic cutoff frequency, in the Kugelwellen formulation, it does not resemble a strict cut off.

A key implication of the throat angle approach is that f_c is not freely chosen, but is instead determined by the geometric constraint imposed by the driver.

Once the profile was fixed, the truncation parameter ξ was selected such that the horn curved back approximately 120°.

The resulting Kugelwellen profile is shown in fig. 5.2.

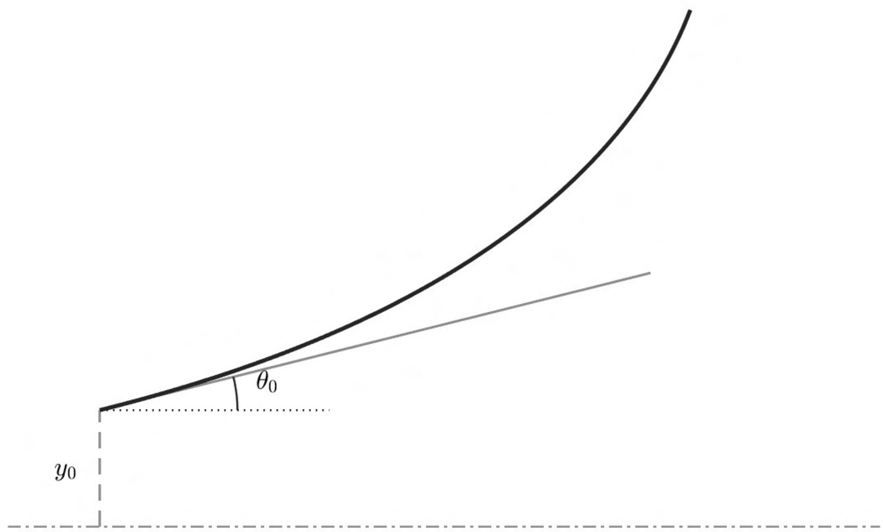

Figure 5.1: Definition of wall half-angle.

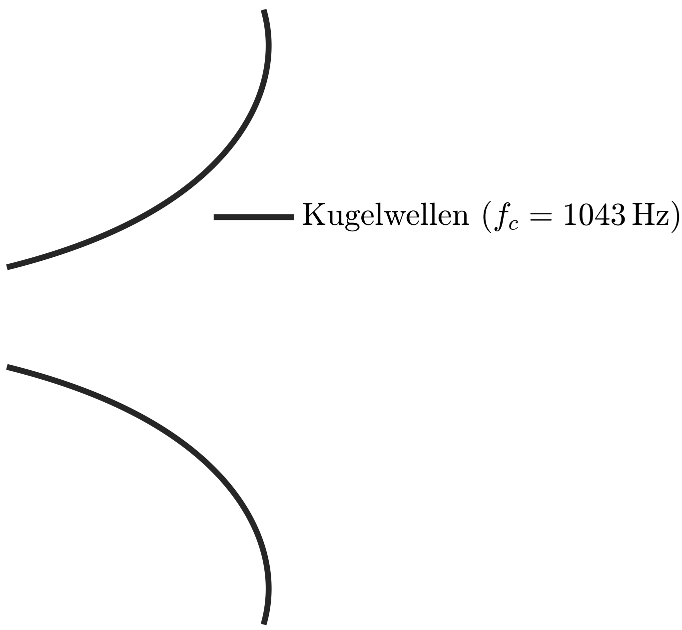

Figure 5.2: Selected Kugelwellen profile

5.3 Oblate Spheroid Parameters

In contrast to the Kugelwellen profile, the oblate spheroid (OS) horn offers significantly greater design freedom. Parameters such as horizontal and vertical coverage angles, profile depth, and termination geometry must all be selected by the designer.

As a result, the design of an OS horn is not uniquely defined, and an optimized design instead requires a combination of prototyping, measuring, and simulation. The analytical expressions describe the geometry, but do not directly prescribe optimal parameter values. As such, to remain within the scope of this research, the parameters selected in this section were guided by a combination of practical constraints, visual considerations, and expected acoustic behaviour. In particular, it was decided to intentionally design the OS horn to be larger than the Kugelwellen horn in order to investigate how this would affect the ceramic manufacturing process.

The horizontal and vertical half-angles were chosen as 30° and 20°, respectively, corresponding to typical studio monitor directivity.

The OS profile was terminated using a clothoid transition, as the horn was intended to function as an external element rather than being mounted flush within a baffle. A MATLAB script was developed to visualise the effect of parameter changes and support iteration of horn profiles during this phase of the design process, see appendix E.2.

The final clothoid parameters were:

- Target exit angle: 130°
- Clothoid scaling parameter: $A = 40$
- Total horn depth: 100 mm

The resulting profile is shown in fig. 5.3.

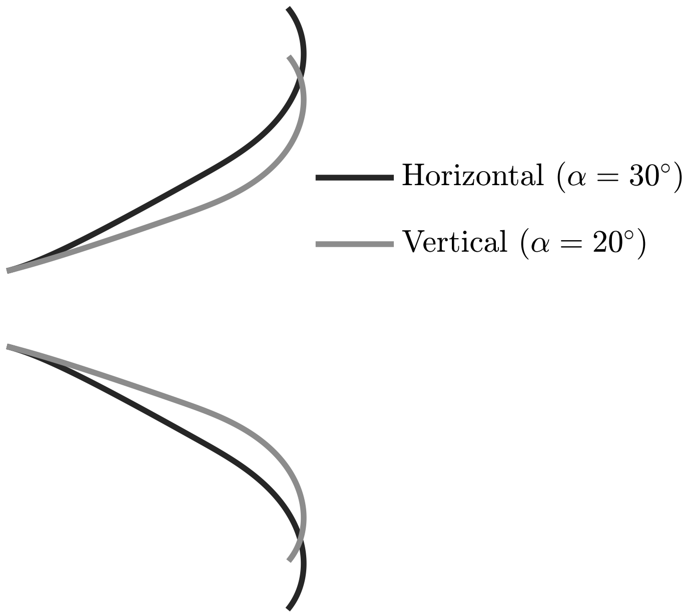

Figure 5.3: Selected OS profiles laid on top of each other

Although Arda Audio typically develops significantly larger horns, smaller prototypes were chosen in this project to reduce manufacturing risk while still allowing meaningful acoustic measurements.

5.4 Further Design of Horns in CAD

The MATLAB-generated curves were imported directly into Creo to preserve their mathematical definition. The outer profiles were constructed using splines, while ensuring curvature continuity. The outer profiles were also designed to follow the conventions of existing horn loudspeaker products on the market. This was partly a practical decision, as the project timeline required moving quickly through the CAD phase in order to leave sufficient time for manufacturing and acoustic evaluation, and partly a reflection of the project's focus on material and manufacturing process rather than geometric innovation.

Initial cross-section designs are shown in fig. 5.4.

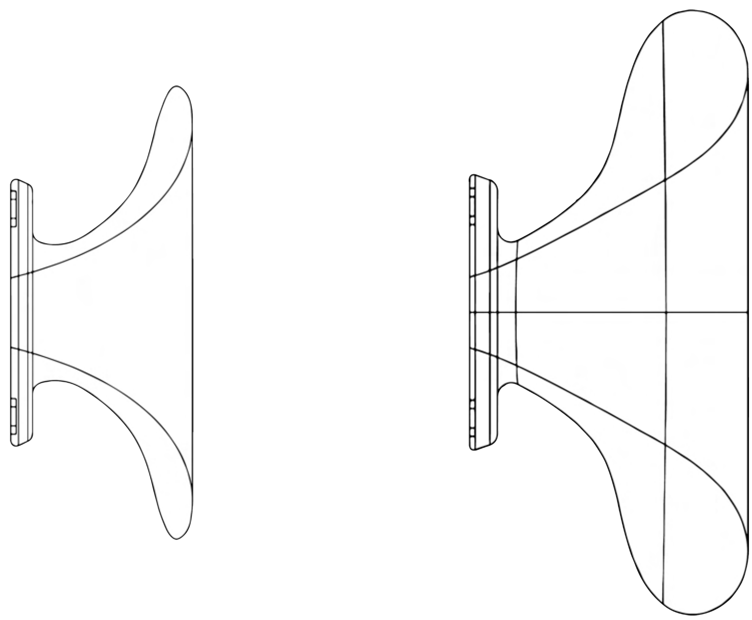

(a) Initial attempt at a Kugelwellen profile. **(b) Initial attempt at an OS horn profile.**

Figure 5.4: Initial horn profile designs.

These early designs were developed under the assumption that solid casting would allow a high degree of geometric freedom. As a result, the cross-sections included substantial variation in wall thickness. While visually expressive, the geometries quickly proved incompatible with the practical constraints of the casting process.

In the OS horn, for example, the thickest regions approached 5 cm, while thinner sections were approximately 1 cm. Such variation introduces several problems. Firstly, during casting, thinner sections can solidify prematurely, forming a “clot” that prevents slip from reaching deeper regions of the mould. Secondly, thick sections significantly increase drying time and increase the risk of non-uniform shrinkage, increasing the likelihood of defects such as cracking or warping.

This constraint demonstrated how ceramic manufacturing fundamentally resists the geometric freedoms often associated with digital fabrication.

The cross-sections were revised reflecting these considerations as shown in figs. 5.5a and 5.5b.

The mounting flange was designed with a thickness of 8 mm for the Kugelwellen horn and 10 mm for the OS horn to provide sufficient structural rigidity.

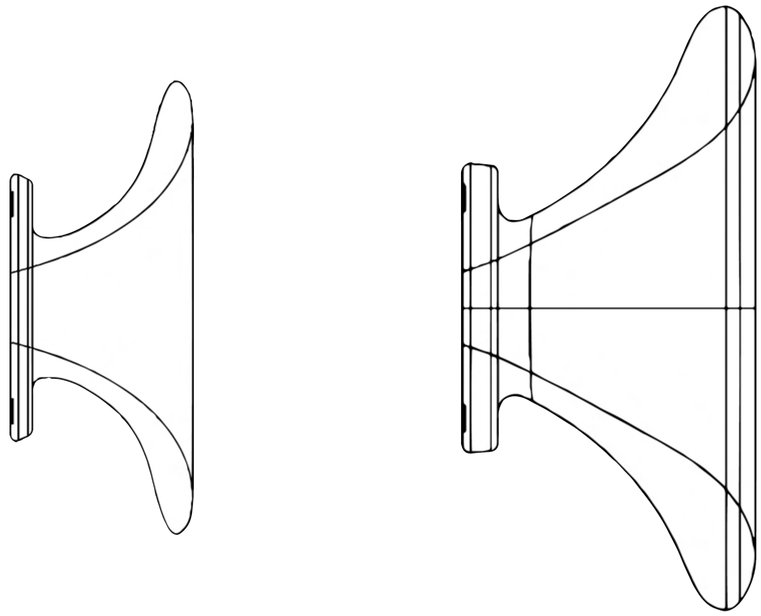

(a) Improved Kugelwellen profile.[1] (b) Improved OS horn profile.

Figure 5.5: Improved horn profile designs.

Oblong indentations were also incorporated into the mounting interface to serve as drill guides for the compression driver mounting screws. These were intentionally designed as oblong rather than circular in order to accommodate small dimensional deviations caused by clay shrinkage during drying and firing.

Draft angles were incorporated throughout the horn geometry to facilitate demoulding. Additionally, matching the exit angle of the compression driver to the horn geometry resulted in an internal draft angle of 38°, further improving mould release.

5.5 Mould Design in CAD

Building on the conceptual sketches, the moulds were fully developed in Creo using the mould cavity feature, which allowed the plaster mould parts to be generated directly from the horn geometry.

[1]Only minor adjustments were made to the Kugelwellen cross-section.

5.5.1 Shrinkage

The mould geometry was scaled to account for clay shrinkage. For this project, two different clay bodies were used. An anthracite stoneware slip was used for the Kugelwellen horn and a white S20 stoneware was used for the oblate spheroid horn [28, 29]. Stoneware was selected over porcelain due to its lower shrinkage rate, reducing the risk of cracking during clay shrinkage around the inner core. The choice to use two different clay bodies was to see if there were any acoustical differences between the two clay bodies.

A shrinkage of 10% was used for both horns based on the manufacturer's specification [28, 29]. Shrinkage was assumed to be isotropic for simplicity.

5.5.2 Plaster Mould Design

Both the Kugelwellen and OS moulds were designed using the same general approach, consisting of four plaster parts depicted in figs. 5.6 and 5.7. The moulds included an internal core forming the inner surface of the horns, two outer halves shaping the exterior geometry, and finally a small plate creating the mounting interface surface.

The mould parts were designed to align during assembly using large locks and keys.

The OS horn mould was split along its major axis to minimise friction during demoulding.

5.5.3 3D Printed Mould Positives

To manufacture the plaster moulds, 3D-printed positives were used. Based on the initial experiments described in section 4.7, the positives were redesigned as components consisting of two primary elements: a face defining the mould surface geometry and a surrounding fence used to contain the plaster during casting.

The fence components incorporated integrated flanges, allowing the assemblies to be clamped together during mould production, see fig. 5.8.

Figure 5.6: Exploded view KW horn

Figure 5.7: Exploded view OS horn

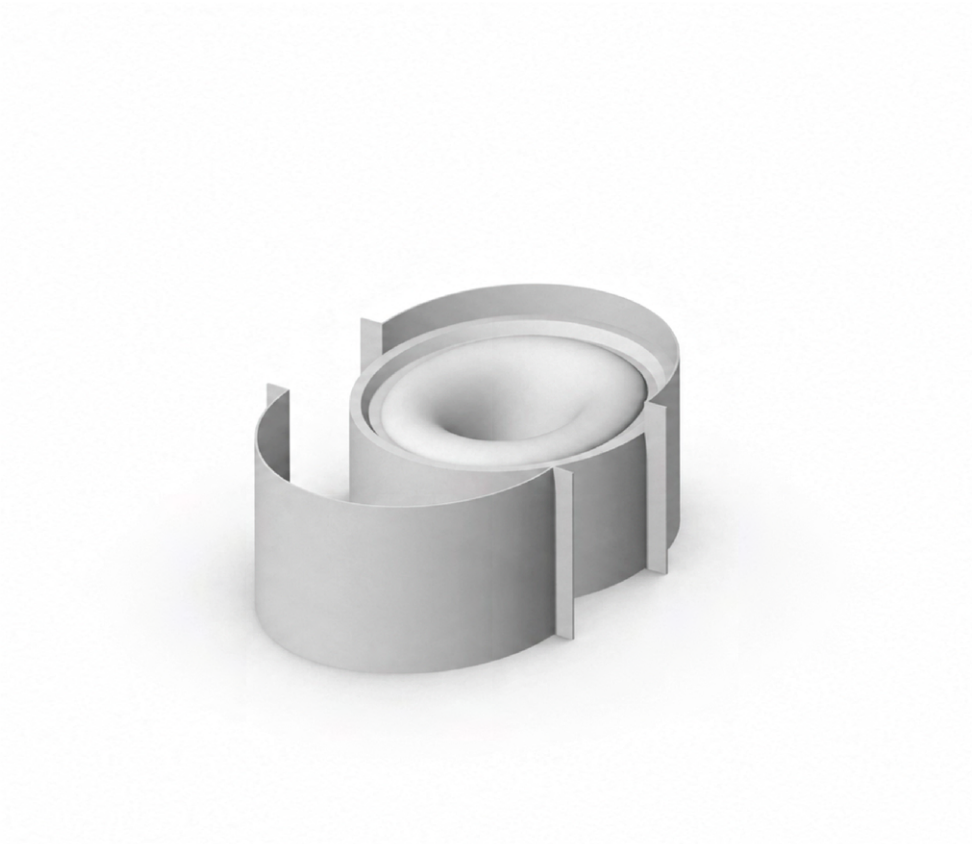

Figure 5.8: 3D printed mould positive showing face and fence

5.5.4 Pour direction

The moulds were designed to be cast with the pour hole located at the throat. This arrangement would simplify post-processing of the horns because the pour hole was placed in an area that would later be concealed by the compression driver. Although this approach contradicted the general recommendation that wall thickness should decrease in the direction of the pour, discussions with Olof Jansson suggested that the thickness variation was moderate enough that successful casting was still likely.

5.6 Reflection on the Detailed Design Phase

The detailed design phase revealed the extent to which ceramic manufacturing constraints directly influenced the development of the horn geometries. While the horn profiles originated as mathematically defined surfaces, their implementation in CAD increasingly became a process of negotiating between acoustic intent, mould feasibility, material behaviour, and structural considerations.

Working on the CAD of the horns made clear how much the lines and overall form matter. How a shape is interpreted as heavy or light, and whether forms should merge or intersect, are decisions that had to be made within a tightly constrained geometric envelope imposed by both the horn profile and the manufacturing process. This made the formal exploration more difficult than anticipated.

More time during the sketching phase should have been spent on the visual character of the horns rather than on mould strategy. Physical or 3D printed models at that stage would have been invaluable, as it is much harder to get a sense of a form from a CAD model alone. A recurring assumption was that time spent on form would be wasted if the acoustic properties of ceramic proved unfavourable. In hindsight, this was incorrect, as explorations in form are material-independent and would have remained relevant regardless of the acoustic outcome.

On the technical side, the OS mould would have benefited from additional keys along its major axis to improve alignment between the two outer halves during assembly.

6 Concept Realisation

This chapter describes the practical manufacturing of the horn prototypes, including 3D printing, plaster mould making, slip casting, firing, and post-processing. As the first physical realisation of the designs, this phase became critical not only for assessing the viability of ceramic horn manufacturing, but also for understanding how the material behaviour of ceramics interacts with digitally developed acoustic geometries. Many of the assumptions established during the CAD phase were tested during manufacturing, revealing the extent to which the final horn geometries remained dependent on mould design, drying behaviour, shrinkage, and practical handling throughout production.

6.1 3D Printing of Mould Positives and Post Processing

The concept realisation began with 3D printing the mould positives. The experiments described in section 4.7 showed that the ability to remove the plaster mould from the printed parts was one of the most critical aspects of the mould-making process. The prints needed to be plaster tight but still flexible to allow for easy demoulding. The following print settings were used:

- Layer height: 0.2 mm
- Wall loops: 2
- Infill: 15%

Although finer layer heights would reduce visible print lines, sanding was required regardless. A standard 0.2 mm layer height was therefore used, with surfaces sanded afterwards to reduce layer lines, see fig. 6.1.

This also highlighted a material trade-off within the workflow. Sanding the printed mould positives inevitably generated plastic dust and microplastic particles, while sufficiently smooth surfaces remained necessary to ensure reliable plaster mould release and reduce surface defects in the final cast components.

Figure 6.1: 3D printed surface postive before and after sanding.

Due to high demand for the university printers and the Easter holiday period, the printing stage took several weeks, delaying the rest of the project. However, the print delays had an unexpected benefit, as they provided additional time to refine the plaster casting process before all parts were available.

6.2 Plaster Casting of Horn Moulds

The printed positives were assembled using binder clips and coated with a plaster mould release agent, see fig. 6.2 [30]. Plaster was mixed using the island method described in appendix B.

Figure 6.2: 3D printed mould positives assembled and ready for plaster casting.

Demoulding the 3D prints remained difficult. In some cases, the plaster needed to be forcefully removed degrading the outer surfaces of the mould. This was not crucial for the slip casting, as the internal surfaces were left undamaged. Still, it reduces the longevity of the moulds and limits the scalability of the manufacturing process.

The mounting-interface indentations proved particularly fragile and were repeatedly damaged, see fig. 6.4. As these were not essential, it was decided to sand them down and replace them later with a separate drilling template described in section 6.3.2.

After demoulding, sharp edges were chamfered to reduce the risk of small pieces of plaster breaking off into the slip, and pour holes were drilled along with air vents see fig. 6.5. The vents were placed around the edges of the mounting interface so that the air could easily escape. The pour hole was made to be 12 mm in diameter, which allowed for an ample flow rate without being excessively large and difficult to clean up during post-processing of the ceramic.

The completed Kugelwellen mould can be seen in fig. 6.6. The moulds were allowed to dry in a drying cabinet for two days before continuing with slip casting.

Figure 6.3: Studio workspace showing 3D printed mould positives filled with plaster.

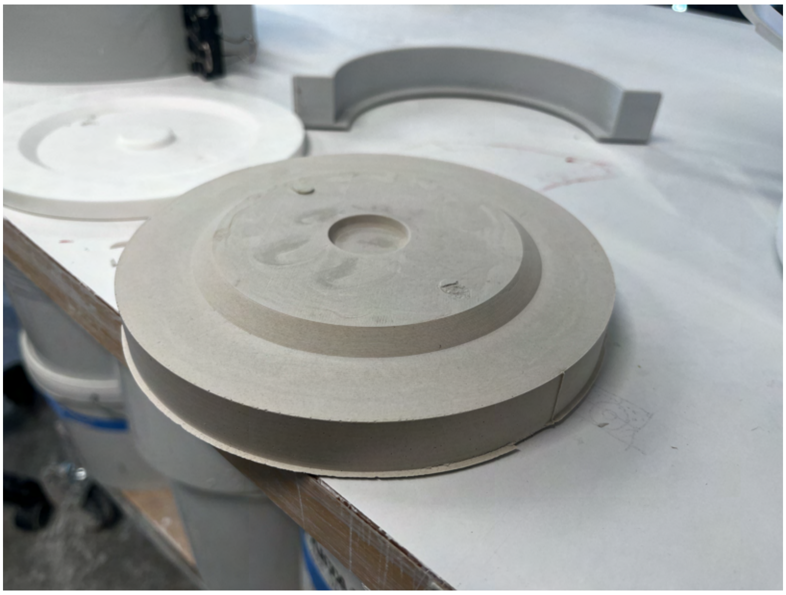

Figure 6.4: Broken mould extrusions.

Figure 6.5: Drilling pour holes.

Figure 6.6: Final Kugelwellen plaster mould.

Figure 6.7: Both horn moulds ready for slipcating.

6.3 Slip Casting Horns

Funnels were 3D printed to fit the pour holes, and the mould sections were held together with rubber bands, see fig. 6.7. The white S20 slip was mixed from powder form before casting. Both slips were strained before being slowly poured into the funnels. This is to ensure that no large particles of slip can get into the mould, resulting in a poorer surface quality.

The slip was poured into the funnel and topped up intermittently for an hour before removing the funnel and letting the mould sit for 24 hours before demoulding. The goal was to keep a continuous flow of slip during the initial hour such that the horns cast solid. The mould was also shaken slightly to remove trapped air bubbles.

Demoulding the green bodies proved simpler than expected, with compressed air sufficient to release them cleanly from the plaster moulds.

6.3.1 Challenges Casting the OS Horn

The Kugelwellen horn was cast successfully on the first attempt. The OS horn proved substantially more challenging. During the first casting attempt, a

Figure 6.8: Mixing slip with a drill before straining it into a separate bucket.

crack formed near the throat, accompanied by an internal bulge presumably caused by trapped air, see fig. 6.9. To try and counteract this defect, a second attempt was made where the horn was shaken and rotated throughout the entire casting to try and spread the slip around the plaster surface. This eliminated the earlier defect but resulted in a hollow mounting flange. The outer walls also easily deformed, indicating hollow walls throughout the horn. This was later confirmed through sectioning of the failed parts. The initial attempt was completely solid, whilst the second attempt contained hollow walls. These hollow walls could be problematic during firing as the expansion of the trapped air could result in the piece cracking or exploding, damaging other pieces in the kiln.

For the third attempt, a second pour hole was added, and the mould was tilted during casting, see fig. 6.10. This approach appeared successful as the resulting green body showed no obvious internal defects. However, due to the earlier setbacks, the third attempt was given insufficient drying time and exploded during bisque firing. This highlighted a characteristic of ceramics as a manufacturing material. Unlike more forgiving processes, it requires significant initial experimentation to understand. Once the variables are controlled however, the process becomes highly repeatable.

Figure 6.9: Crack at the throat of the initial OS attempt.

Figure 6.10: Improved mould setup for casting the OS horn.

6.3.2 Postprocessing Ceramic

After demoulding, the greenware was allowed to dry to the leather-hard state. Seam lines were trimmed with a knife and the surfaces were refined with a damp sponge seefig. 6.11.

Figure 6.11: Seam lines present after demoulding.

After bisque firing, additional sanding was carried out to improve the surface quality, see fig. 6.12.

A separate 3D printed drilling jig was used to ensure that the mounting holes were drilled as accurately as possible, see fig. 6.13.

6.3.3 Glazing and Firing

The Kugelwellen horn was glazed with a brush-on matte black glaze, while the OS horn was finished with a satin white dip glaze. This also provided an opportunity to compare the visual surface quality achievable with the two glazing methods.

The horns were fired to 1260° and held there for 15 minutes before the kiln was allowed to cool off [31].

Even though the shrinkage during glaze firing had been considered when

Figure 6.12: Sanding of bisqueware.

creating the drill template, the holes in the mounting flange still needed to be adjusted with a diamond file after firing.

6.4 Reference Horns

The 3D printed reference horns were printed in PLA using print settings guided by Arda Audio. Following Tsvetan's assessment that variations in print settings would have negligible acoustic influence, a single set of reference horns was produced. The reference horns were sanded smooth to avoid introducing additional variables into the measurements. The following print settings were used:

- Layer height: 0.2 mm
- Infill: 15% gyroid
- Wall perimeters: 3

Figure 6.13: 3D printed drill template used for drilling bisqueware.

6.5 Resulting Horn Prototypes

The glazing on the OS horn became uneven and thin, presumably due to rushing during the dipping process. Rather than attempting a second glaze firing, it was decided to proceed with the existing prototype, as the acoustic performance remained unknown at this stage and the OS horn had already been identified as requiring a redesign for production. Aside from the glaze quality, the final OS horn closely matched the CAD model in geometry.

The Kugelwellen horn achieved a high quality surface finish, though a slight irregularity in the curvature around the mouth remained. The dip glaze used on the OS horn produced a marginally smoother surface to the touch than the brush-on glaze applied to the Kugelwellen horn.

Both horns showed minor dimensional deviation at the mouth relative to the CAD model. The throat diameters of the finished ceramic Kugelwellen and OS horns were 26.08 mm and 25.52 mm respectively, against a target of 25.4 mm (1 inch). This represents a close agreement with the intended dimensions, indicating that the shrinkage compensation was well-calibrated. The greater accuracy at the throat compared to the mouth is consistent with linear shrinkage behaviour: the throat sits closer to the central axis of the horn, and therefore moves less in absolute terms during shrinkage than the mouth,

Figure 6.14: Final OS horn prototype.

Figure 6.15: Final Kugelwellen horn prototype.

which is further from the axis.

6.6 Reflection on the Concept Realisation Phase

The concept realisation phase demonstrated that ceramic horn manufacturing is feasible, but highly sensitive to mould design, air entrapment, and drying conditions. The results suggest that thick-walled castings introduce more manufacturing complexity than may be warranted, while also contributing to geometries that, particularly in the case of the OS horn, read as visually heavy. Thinner wall sections could therefore both simplify production and better exploit the aesthetic potential of the material. However, the extent to which thinner geometries may introduce additional risks of warping was not explored within the scope of this project.

Several process improvements were identified. Using flexible shells for the mould positive faces rather than solid blocks would allow the prints to be flexed during demoulding, perhaps reducing surface degradation. This would also enable thermal demoulding, where a cold substance such as rubbing alcohol is introduced into the shell to exploit the shrinkage of the PLA for release.

A modular mould system, where components such as the clothoid termination can be swapped out independently, would also significantly reduce the effort required to iterate on horn geometry.

Shrinkage compensation could be further improved by controlling the specific gravity of the slip prior to casting, as shrinkage is sensitive to water content and will vary between batches without this control. This would also allow the drill jig to be refined to more precisely account for glaze firing shrinkage.

Casting in porcelain, and potentially pigmenting the slip, would open up a wider range of formal and chromatic expressions more closely aligned with Arda Audio's existing product range. That said, the visual outcome was not the primary objective of this phase, which was intended as an initial feasibility study rather than a resolved design proposal.

7 Acoustical Evaluation

The purpose of the acoustical evaluation was to compare ceramic horns with geometrically equivalent 3D printed reference horns. The measurements were intended to determine whether the increased stiffness and mass of ceramic materials produce measurable differences in frequency response, directivity, and harmonic distortion. This phase also provided insight into the practical realities of acoustic testing within small-scale development environments, where access to specialised facilities may be limited and measurement workflows must often be adapted to available spaces and equipment.

7.1 Design of Experiments

The experimental methodology was designed to isolate the influence of material. For each horn geometry, a ceramic horn and a 3D-printed reference horn were mounted to the same compression driver and measured under what aimed to be identical conditions.

The two horn geometries evaluated were the Kugelwellen horn and oblate spheroid horn.

For each geometry, the ceramic horn and 3D-printed PLA reference horn were measured resulting in four test specimens in total.

The following acoustic characteristics were measured:

- On-axis frequency response
- Off-axis frequency response
- Total harmonic distortion (THD)

Each measurement was repeated three times to assess repeatability and precision.

7.2 Measurement Equipment

The measurements were conducted using the following equipment:

- Measurement microphone: Dayton Audio EMM-6 with calibration file
- Audio interface: Focusrite Scarlett 2i2 (3rd generation)
- Power amplifier
- Compression driver: BMS 4550
- Passive second-order high-pass filter
- Computer running Room EQ Wizard (REW)
- Loudspeaker stand or fishing line suspension
- Ceramic horn prototypes
- 3D-printed PLA reference horns
- Various cables

7.3 Protection Filter Design

To protect the compression driver from low-frequency noise, a passive second-order Butterworth high-pass filter was designed and placed between the amplifier and the driver. The filter design and calculations are provided in appendix F.

Although REW generates band-limited sweep signals, the additional analog filter provides protection against low-frequency noise that may originate from the computer, audio interface, or amplifier.

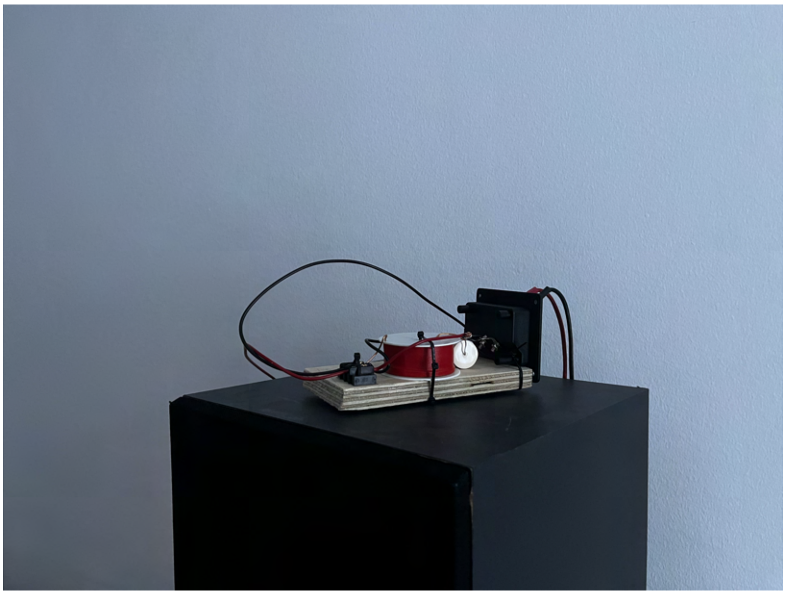

Figure 7.1: Constructed second-order Butterworth high-pass filter used to protect the compression driver.

7.4 Measurement Setup

All measurements were carried out in the anechoic chamber at HUMLAB, Lund University. While the chamber provided a controlled acoustic environment with minimal reflections, it was not specifically designed for loudspeaker measurements, which introduced several practical limitations during testing.

Prior to testing, the voltage levels in REW were calibrated using a multimeter at the amplifier terminals and the Focusrite Scarlett 2i2 was also calibrated using REW's soundcard calibration feature. The calibration file supplied with the Dayton Audio EMM-6 microphone was imported into REW. After calibration, the interface gain remained unchanged throughout all measurements to maintain consistent relative excitation levels.

The microphone was positioned at a fixed distance of 1 m from the horn mouth.

The horn and compression driver assemblies were suspended using fishing line attached to hooks in the ceiling of the anechoic chamber. This approach was chosen in an attempt to minimise unwanted resonances and reflections that could arise from using a conventional loudspeaker stand. However, the suspension system introduced several practical challenges related to alignment and positioning repeatability.

For most horn configurations, the compression driver caused the assembly to become back-heavy, allowing stabilising fishing lines to be attached below the horn. This arrangement is shown in fig. 7.2. However, the ceramic oblate spheroid horn was significantly front-heavy, requiring additional suspension lines attached directly above the horn mouth. As a result, one fishing line passed directly in front of the horn mouth, as shown in fig. 7.3a. It was assumed that the fishing line was thin enough that it would produce negligible acoustic influence, although this remains a potential source of uncertainty. The suspension system was assembled using fishing lines, carabiners, and zip ties, shown in fig. 7.4.

An advantage of the ceiling hook arrangement was that the hooks were positioned approximately 45° apart, which simplified the positioning of the off-axis measurements.

Figure 7.2: Side view of the suspended horn measurement setup.

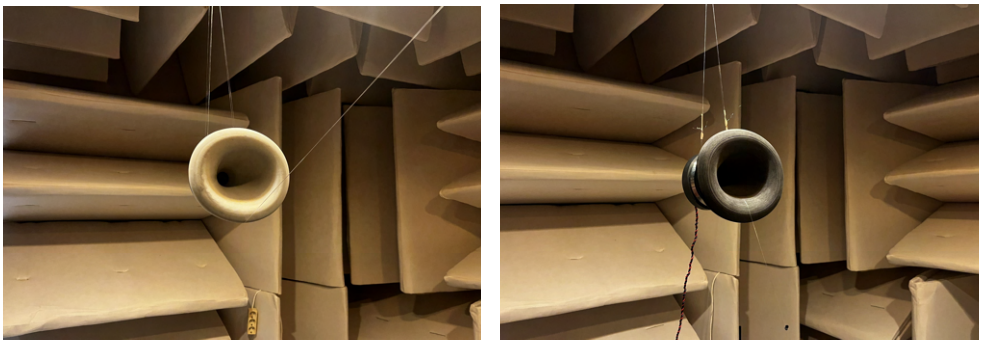

(a) Ceramic oblate spheroid horn **(b) PLA oblate spheroid horn**

Figure 7.3: Different suspension arrangements used during measurements.

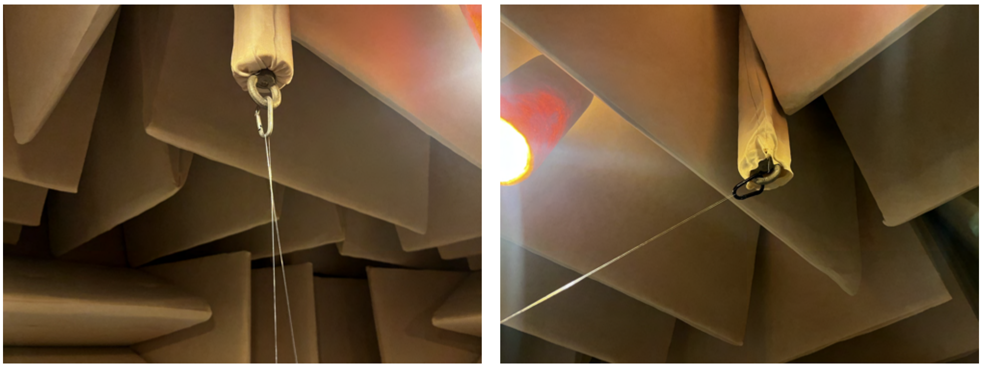

Figure 7.4: Fishing line mounting details using carabiners and zip ties.

Figure 7.5: Measurement setup used in the anechoic chamber.

7.5 Excitation Level

Absolute sound pressure level calibration was not available. Instead, all measurements were performed at a constant drive voltage in order to allow meaningful relative comparisons between horn configurations.

The amplifier output voltage was adjusted to 2.83 V_{RMS} which corresponds to approximately 1 W into an 8 Ω load.

This drive level was selected as a compromise between obtaining sufficiently strong measurement data while remaining below the rated power handling limits of the BMS 4550 compression driver when operated above the recommended crossover frequency.

Using a fixed voltage ensures that all comparisons are made under identical excitation conditions, allowing valid direct comparisons even without absolute SPL calibration.

7.6 Frequency Response Measurements

7.6.1 On-Axis Measurements

On-axis measurements were performed with the microphone positioned directly in front of the horn mouth.

A logarithmic sine sweep from 600 Hz to 22 050 Hz was used for all measurements. The lower limit was intentionally placed below the recommended crossover frequency of the BMS 4550 in order to observe both the horn roll-off behaviour and the response of the protection filter.

Each horn configuration was measured three times. Between repetitions, the horn was removed and remounted to the compression driver. This was done to incorporate assembly variability into the measurements and reduce the likelihood that results were overly dependent on a single mounting condition.

7.6.2 Off-Axis Measurements

Off-axis measurements were conducted by rotating the horn relative to the microphone while maintaining a constant microphone distance.

The off-axis angle used during measurements was approximately 45°.

The same sweep settings and repetition procedure used for the on-axis measurements were retained for the off-axis measurements.

Because the ceiling hooks and floor directly underneath them were used throughout testing, the relative positioning between measurements was expected to remain reasonably repeatable, although some uncertainty remained due to movement within the suspension system.

7.7 Total Harmonic Distortion

Total harmonic distortion (THD) measurements were performed on-axis using the same excitation level and sweep settings as the frequency response measurements.

7.8 Measurement Sequence

To reduce systematic error, the measurement order was alternated between materials and geometries.

A typical sequence was:

1. Ceramic Kugelwellen horn
2. PLA Kugelwellen horn
3. Ceramic oblate spheroid horn
4. PLA oblate spheroid horn

By alternating configurations rather than measuring all repetitions of one horn consecutively, variations in equipment behaviour or mounting conditions were distributed across all specimens.

7.9 Data Processing

Raw measurement data was exported from REW and processed in MATLAB. For each configuration, the three repeated measurements were averaged point-by-point across frequency. Standard deviation was calculated simultaneously in order to visualise repeatability and identify regions where mounting or positioning variations may have influenced the measurements.

Because absolute SPL calibration was unavailable, all frequency response data was normalised relative to a common reference level. This allowed meaningful comparison between horn materials and geometries while preserving the relative differences between on-axis and off-axis measurements.

A $\frac{1}{6}$ octave smoothing was applied to frequency response measurements, while THD data was smoothed using a $\frac{1}{3}$ octave in accordance with common loudspeaker measurement practice [16].

7.10 Measurement Reliability and Limitations

Several steps were taken to improve reliability as mentioned previously. Despite these precautions, several limitations remained.

The suspension system made it difficult to guarantee perfectly repeatable positioning, particularly the off-axis measurements were sensitive to small movements within the suspension system. This was especially noticeable for the ceramic oblate spheroid horn, which exhibited greater positional instability during testing and may therefore show increased measurement variation

Another limitation was the inability to position the microphone perfectly on-axis relative to the horn mouth due to the physical constraints of the chamber setup, shown in fig. 7.6.

Lastly, ceramic shrinkage during firing introduced dimensional uncertainty between the ceramic and PLA horns. Surface finish differences between the glazed ceramic surfaces and layered PLA prints may also have influenced the results to some extent.

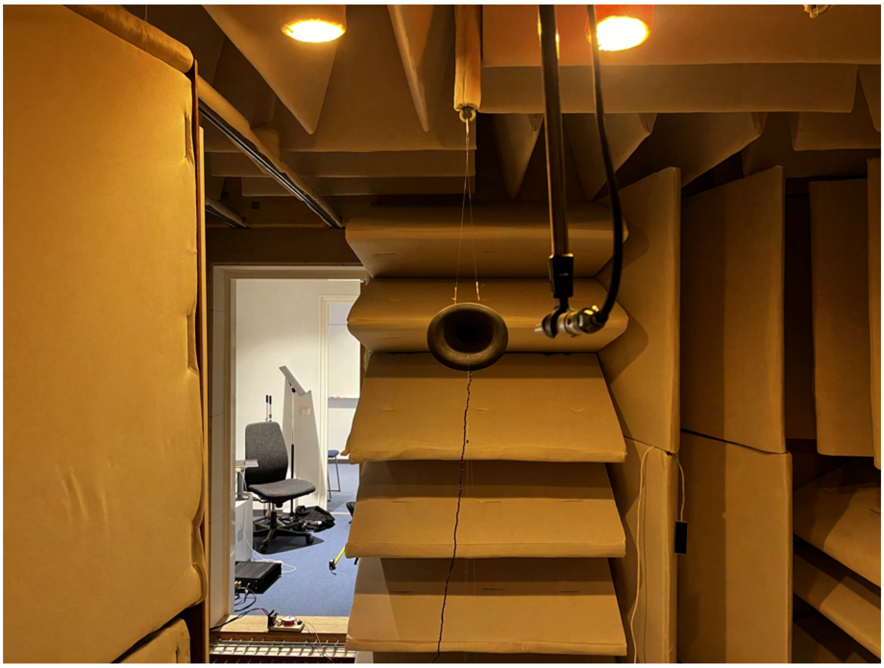

Figure 7.6: Front view of the measurement setup illustrating microphone alignment limitations.

7.11 Reflection on Experimental Method

The methodology developed in this thesis represents a compromise between experimental control and the practical realities of exploratory small-scale loudspeaker development. While the setup lacks some of the precision associated with industrial loudspeaker testing facilities, the use of repeated measurements, controlled excitation levels, and an anechoic environment provides a sufficiently robust basis for relative comparison between horn materials.

An important aspect of this project was not only the acoustic evaluation itself, but also understanding how such experiments can realistically be carried out within the context of independent design practice and small-scale manufacturing. The process therefore reflects the broader themes of the thesis: experimentation, material exploration, and the intersection between engineering precision and hands-on making.

7.12 Results

7.12.1 On-Axis Frequency Response

7.12.1.1 Kugelwellen Horn – Ceramic vs. PLA

The measured on-axis responses of the ceramic and PLA Kugelwellen horns were highly similar across the full measured frequency range. Both horns exhibit a broad increase in output centred around approximately 1.5 kHz, followed by a gradual reduction in level towards higher frequencies. A small dip is visible around 3–4 kHz in both measurements.

The standard deviation bands remain narrow throughout the measured range, indicating good repeatability between measurements and relatively low sensitivity to mounting variations for this horn geometry.

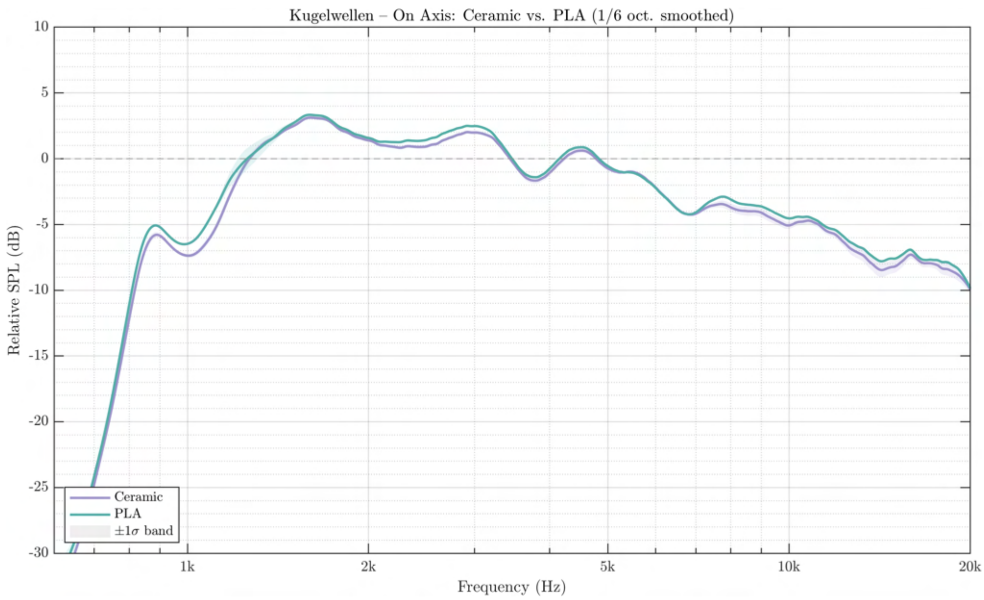

Figure 7.7: Kugelwellen horn – on-axis frequency response for ceramic and PLA horns (1/6 octave smoothing).

7.12.1.2 Oblate Spheroid Horn – Ceramic vs. PLA

The ceramic and PLA oblate spheroid horns also exhibit highly similar on-axis responses. Compared to the Kugelwellen horns, both oblate spheroid horns display a flatter overall response through much of the midrange frequencies.

Small differences begin to appear above approximately 10 kHz, where the ceramic horn maintains marginally higher output than the PLA version. However, the magnitude of this difference remains relatively small compared to the overall variation of the measurements.

The standard deviation bands are again relatively narrow, although slightly wider than those observed for the Kugelwellen horns.

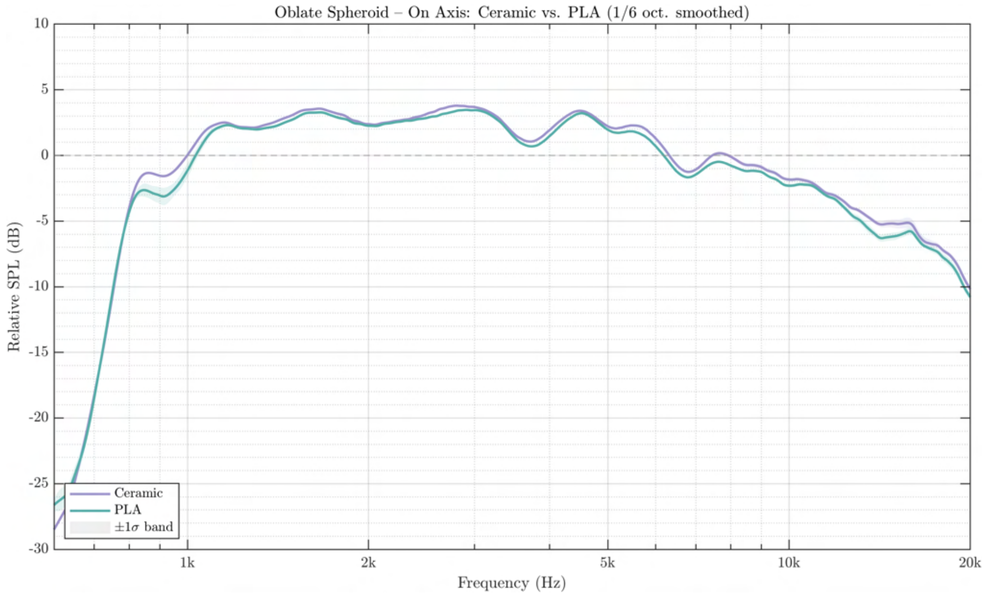

Figure 7.8: Oblate spheroid horn – on-axis frequency response for ceramic and PLA horns (1/6 octave smoothing).

7.12.2 Off-Axis Frequency Response

7.12.2.1 Kugelwellen Horn – Ceramic vs. PLA

The off-axis responses of the ceramic and PLA Kugelwellen horns remain closely matched throughout the measured range. Both horns display a gradual reduction in output towards higher frequencies, consistent with increasing directivity at shorter wavelengths.

Differences between the two material variants remain small and generally fall within the standard deviation bands.

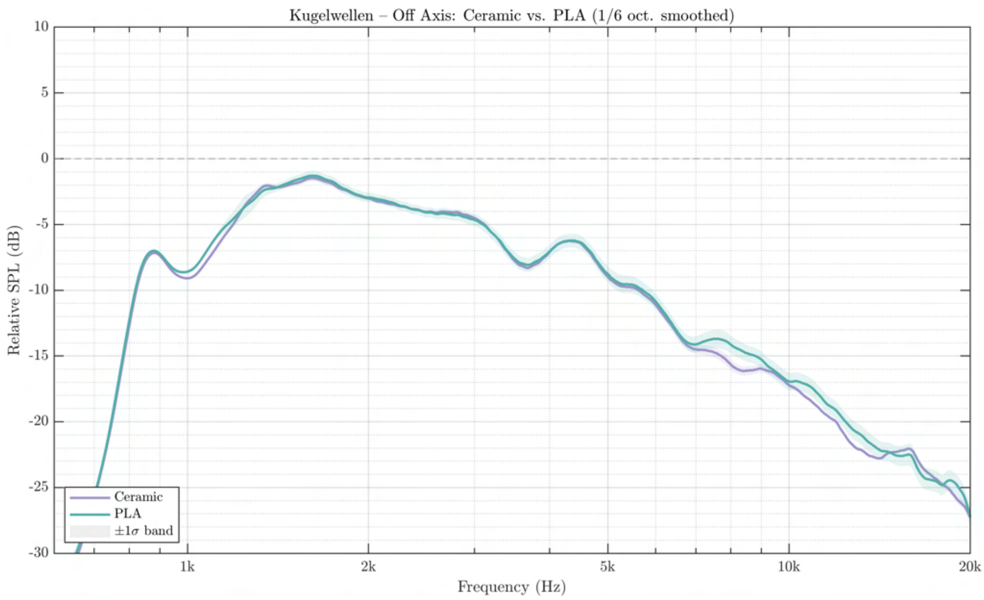

Figure 7.9: Kugelwellen horn – off-axis frequency response for ceramic and PLA horns (1/6 octave smoothing).

7.12.2.2 Oblate Spheroid Horn – Ceramic vs. PLA

The oblate spheroid horns display somewhat larger differences between ceramic and PLA during the off-axis measurements. The ceramic horn maintains slightly higher output through parts of the midrange and high-frequency region, while the PLA horn exhibits a steeper roll-off towards higher frequencies.

The ceramic oblate spheroid horn also displayed the widest standard deviation bands of all measured configurations, particularly above approximately 5 kHz.

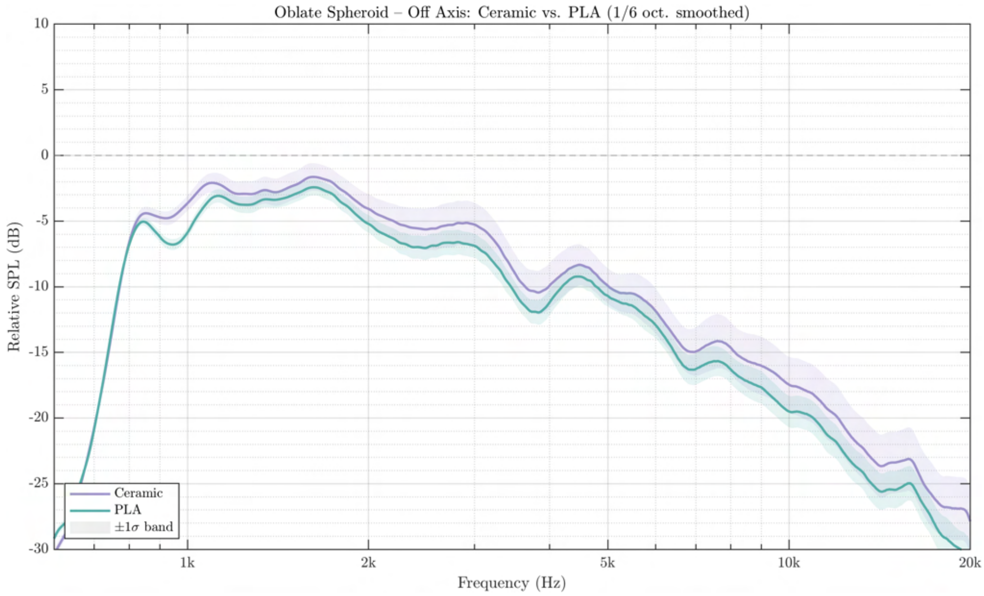

Figure 7.10: Oblate spheroid horn – off-axis frequency response for ceramic and PLA horns (1/6 octave smoothing).

7.12.2.3 Comparison Between Horn Geometries

When comparing the two horn profiles directly, larger differences become apparent than those observed between material variants.

The oblate spheroid horns generally exhibit flatter off-axis behaviour through the lower and mid frequency ranges, while the Kugelwellen horns maintain relatively higher output at higher frequencies.

The low-frequency behaviour also differs between the horn geometries. The Kugelwellen horns exhibit a more pronounced reduction in output below approximately 1 kHz, while the oblate spheroid horns begin their low-frequency roll-off more gradually.

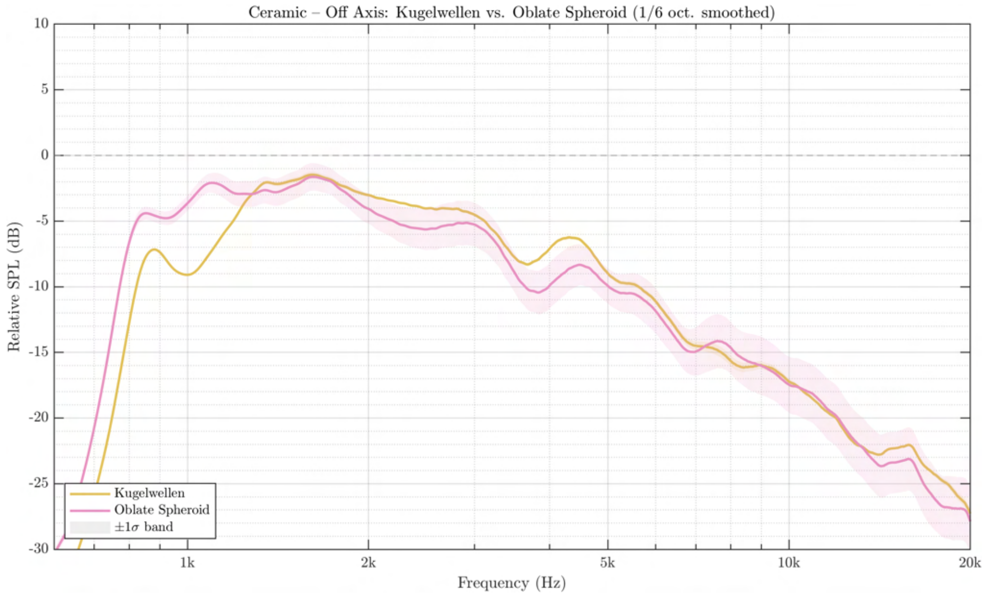

Figure 7.11: Ceramic horns – off-axis comparison between Kugelwellen and oblate spheroid geometries (1/6 octave smoothing).

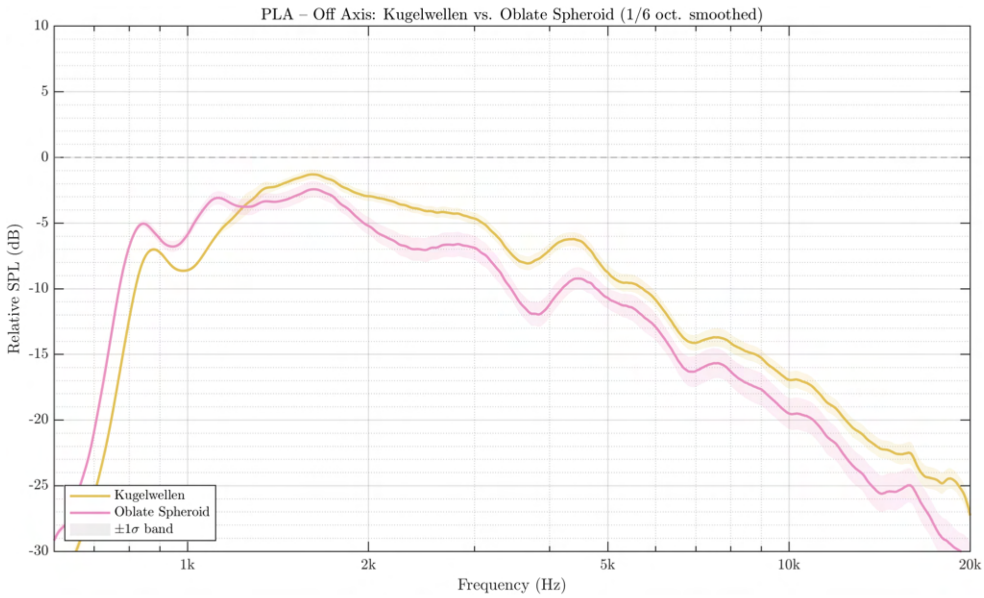

Figure 7.12: PLA horns – off-axis comparison between Kugelwellen and oblate spheroid geometries (1/6 octave smoothing).

7.12.3 Total Harmonic Distortion

7.12.3.1 Kugelwellen Horn – Ceramic vs. PLA

The THD measurements for the Kugelwellen horns show very similar behaviour between the ceramic and PLA variants.

Distortion is highest at low frequencies, decreases rapidly above approximately 1 kHz, and then rises again moderately through parts of the midrange before gradually decreasing towards higher frequencies.

The ceramic horn exhibits marginally lower distortion near the minimum region around 1 kHz, although the difference remains relatively small.

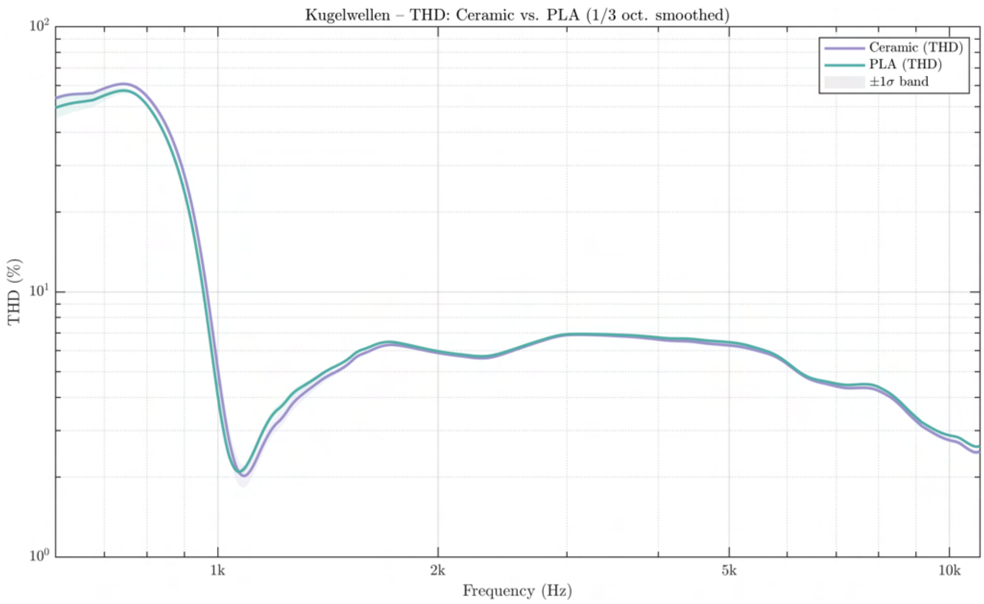

Figure 7.13: Kugelwellen horn – total harmonic distortion for ceramic and PLA horns (1/3 octave smoothing).

7.12.3.2 Oblate Spheroid Horn – Ceramic vs. PLA

The oblate spheroid horns display a similar overall THD behaviour to the Kugelwellen horns, although with a slightly different distortion profile through the midrange frequencies.

The ceramic and PLA variants again track closely throughout most of the measured range.

Relatively high distortion levels remain present through portions of the measured frequency range, including frequencies above the expected horn cutoff region.

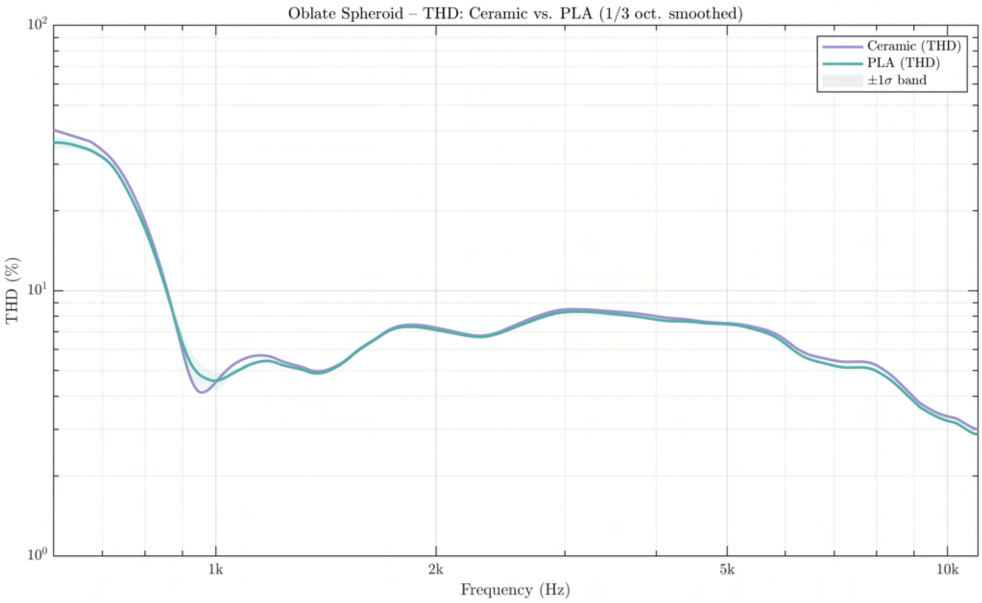

Figure 7.14: Oblate spheroid horn – total harmonic distortion for ceramic and PLA horns (1/3 octave smoothing).

7.13 Interpretation of Results and Discussion

Across all measurements, horn geometry exerted a larger influence on acoustic behaviour than horn material. Differences between ceramic and PLA horns were consistently small, particularly for the on-axis frequency response measurements, where most variations remained within the standard deviation bands. This suggests that within the conditions of this experiment, the choice of horn material has a limited influence on the measured frequency response compared to the influence of horn profile geometry.

The largest observable differences between material variants occurred in the off-axis measurements of the oblate spheroid horns, where the ceramic horn maintained slightly higher output through parts of the midrange and exhibited a less steep high-frequency roll-off compared to the PLA version. However, these measurements also produced the widest standard deviation bands of all configurations tested. This is likely connected to the physical setup of the oblate spheroid ceramic horn, which, due to its different weight distribution, required an alternative suspension arrangement in which it was attached to the hooks in the ceiling of the anechoic chamber, as described in section 7.4. This arrangement made it more difficult to ensure consistent off-axis angles between repetitions, and may therefore account for at least part of the observed difference between ceramic and PLA for this configuration. As such, the material-related contribution cannot be fully separated from this measurement uncertainty.

The differences between the Kugelwellen and oblate spheroid geometries were considerably larger than the differences between ceramic and PLA variants of the same geometry. This was apparent in both the on-axis and off-axis measurements, and is consistent with theoretical expectations: horn profile geometry governs the flare rate, the cutoff frequency, and the directivity behaviour of the horn, and these factors produce measurable and predictable differences in acoustic output. Material properties such as stiffness and internal damping would primarily affect the structural vibration behaviour of the horn walls, which would only be expected to produce second-order effects on the radiated sound field.

The THD measurements require careful interpretation. Elevated distortion below the horn cutoff frequency is expected due to reduced acoustic loading of the compression driver diaphragm in this region, and the steep rise below approximately 800 Hz visible in all measurements is consistent with this behaviour. However, the distortion levels measured above 1 kHz, where the driver operates within its intended frequency range, were approximately 5–7 % across all configurations. For a professional compression driver operating at 1 W into an 8 Ω load, distortion within the passband would typically be expected to remain below 1–2 % under well-controlled conditions [16]. The measured values are therefore elevated relative to what a well-performing system of this type would normally produce. It should be noted that the BMS 4550 datasheet does not publish a THD specification, making direct comparison against manufacturer claims impossible.

Critically, the THD behaviour was nearly identical across all four horn configurations throughout the measured frequency range, with ceramic and PLA variants tracking each other closely for both horn geometries. If distortion were influenced by horn wall resonances or material-related non-linearities, different material variants would be expected to exhibit measurably different distortion profiles. The near-identical THD curves across all configurations therefore strongly suggest that the distortion originated in the compression driver itself rather than in the horn walls. Possible contributing factors include the excitation voltage of 2.83 V_{RMS} being relatively high for near-cutoff operation, or mechanical non-linearities within the diaphragm assembly. A measurement at reduced drive levels, or using a calibrated plane wave tube, would help isolate the contribution of the driver from any horn-related effects in future work.

Overall, the results do not provide strong evidence that ceramic horn construction produces substantially different acoustic behaviour compared to geometrically equivalent PLA horns under the conditions tested. Small differences in high-frequency and off-axis behaviour may reflect some secondary influence of material stiffness or surface properties, but these effects are small relative to the influence of horn geometry and, in some cases, relative to the measurement uncertainty introduced by the experimental setup.

7.14 Further Development

Several areas could be explored further in future work. More controlled mounting fixtures could significantly improve repeatability, particularly for off-axis measurements. A dedicated rotational measurement rig would likely reduce positioning uncertainty considerably. Future work could also investigate other ceramic formulations, wall thicknesses, or internal damping treatments in order to explore whether stronger material-related acoustic differences can be observed.

Further testing needs to be done on how the ceramic horn behaves at various thicknesses compared to the PLA. As concluded in section 6.6, slip casting thinner ceramic forms could improve the production process. It was assumed that very thin-walled ceramic horns would ring a lot at high frequencies, but the results from this acoustical evaluation suggest this may not be as big an issue. It would also be interesting to see how they would compare when placed in a baffle and maybe see how the super elliptical termination could be used for the oblate spheroid horn.

8 Discussion

Somewhere during the design phase, this project quietly changed shape. What had started as a question about acoustic material differences became, in practice, an investigation into what it takes to bring a mathematically defined form into existence in clay.

The acoustic evaluation gave a relatively clear answer. Within the conditions of the experiment, horn geometry exerted a substantially greater influence on acoustic behaviour than horn material. Differences between ceramic and PLA variants of the same profile were small and, in most cases, fell within measurement uncertainty. This outcome was perhaps surprising given the significant differences in stiffness and density between the two materials. One might have expected ceramic wall resonances to leave a visible signature in the frequency response or distortion measurements. That they did not, or at least not measurable with the available setup, is itself a meaningful result, and one that aligns with the theoretical expectation that horn wall behaviour produces only second-order effects on the radiated sound field under normal operating conditions.

What this finding does not resolve is whether the result would hold for thinner ceramic walls, where the reduced mass might allow structural resonances to introduce a measurable difference in performance. The thick walls were partly a consequence of wanting to explore solid casting, and partly a response to a concern raised by several people during the project, that ceramic horns would ring badly and colour the sound in ways that would make them acoustically unviable. Thicker walls felt like a way to guard against that and as such the forms were also still shaped by what existing horns on the market look like, rather than by what ceramic on its own terms might produce. The acoustic results suggest those fears may have been overstated, which makes the caution feel somewhat misplaced in hindsight, and raises the question of whether the design was more cautious than it needed to be. A thinner horn, or one that engaged more seriously with what distinguishes ceramic as a form-giving material, might have been more acoustically interesting to study and more formally distinct as an object.

More practically, the acoustic result means that the case for ceramic horns does not rest on measurable performance advantages, at least not at this scale and wall thickness. Instead it rests on the qualities that ceramics offer as a material: surface character, visual weight, the depth of finish that glazing allows, and a sense of permanence that printed polymers rarely convey. These are not acoustic arguments, but they are legitimate artistic arguments, and they are consistent with the kind of thinking that motivates small-scale manufacturers like Arda Audio. In this sense, the acoustic finding is not a failure of the premise, it is a clarification of it.

The manufacturing process proved to be the more complex and, ultimately, more interesting outcome of the project. What began as a method for producing a horn became, over the course of the work, a system in its own right: a chain of decisions about mould geometry, parting lines, pour strategy, clay body selection, drying, and firing, each of which constrained the next. The shift described in Chapter 3, from designing a horn to designing a process for producing one, was not planned, but it reflects something genuine about material-driven design. When a material imposes real constraints, the design process becomes a negotiation rather than an execution.

Working with ceramics required accepting a degree of unpredictability that is somewhat absent from polymer 3D printing. Cast-to-cast variability, in wall uniformity, surface quality, and dimensional accuracy after firing, is inherent to the process. The oblate spheroid horn required three casting attempts before a structurally sound green body was achieved, and even then the glaze firing introduced further variation. This variability is not simply a problem to be solved through better technique, although technique matters. It is a property of the material and the process, and any serious attempt to use slip casting in a small-scale production context must account for it. A single horn produced to a high standard is achievable; consistent production of multiples requires a level of process refinement that was outside the scope of this project. This also means the process as it stands does not map neatly onto the rapid prototyping workflow that currently defines Arda Audio's development cycle, where iteration speed is a core advantage. Whether ceramics could complement that workflow, as a finishing material for selected designs once a geometry has been validated in PLA, for instance, is a more realistic framing than a direct replacement, and one that might bring something genuinely new to the product range.

This connects to a broader question that runs through the thesis: what does small-scale ceramic production actually require, and who is it realistic for? The workflow developed here, mathematical profile generation, CAD modelling, 3D-printed mould positives, plaster casting, and kiln firing, draws on a wide range of skills and access to equipment that is not universally available. The specific tools used in this project, MATLAB and Creo, carry significant licence costs, but free and low-cost alternatives exist: Python with standard numerical libraries can reproduce the profile generation scripts without modification, and capable CAD environments are available at low cost or for free. The barrier is less about capital than about accumulated knowledge: understanding how clay behaves, how plaster moulds absorb water, how drying conditions affect the final piece. This kind of knowledge is hard to acquire quickly, but it is transmissible and it exists in communities of practice that are accessible to designers willing to engage with them.

The project was, in this sense, as much about learning a material as it was about producing a product. This report has tried to document that process honestly and as such documented an entirely imperfect method. That transparency is deliberate. A documentation that showed only the finished horns would obscure the most practically useful information: where the process is fragile, where it requires judgement rather than just procedure, and where future work should focus. The ceramic horns that resulted are preliminary, prototypes in the genuine sense, not finished objects. But the process that produced them is documented, understood to a useful degree, and improvable. That feels like the more durable outcome.

9 Conclusion

The acoustic measurements gave a relatively clear answer to the third research question: within the conditions of this experiment, horn material did not produce measurable differences in acoustic performance comparable to those produced by horn geometry. Ceramic and PLA variants of the same profile behaved similarly across all measured parameters. The first two research questions are harder to answer cleanly. A feasible manufacturing process was developed and documented, and a small number of successful prototypes were produced. Whether this process is viable for small-scale production depends heavily on how viability is defined. As a one-off making process, it works. As a repeatable workflow, it requires a level of process refinement that was outside the scope of this project, and ceramics, as a material, demands significant initial experimentation before consistent results can be achieved.

What this project has established is a foundation. The mathematical profile generation, mould design strategy, and casting approach are all documented and improvable. Several directions stand out as particularly worth pursuing. Thinner-walled ceramic horns may reduce manufacturing complexity and produce more acoustically interesting results. Casting in porcelain, rather than stoneware, would open up a wider range of formal and surface expressions. A more controlled measurement setup, a dedicated rotation rig rather than a suspended fishing line arrangement, would allow more reliable off-axis characterisation.

More broadly, the workflow developed here suggests that combining digital fabrication with traditional ceramic forming is a realistic option for small studios willing to invest in the process knowledge it requires. That investment requires collaboration with people who understand the material, but the outcome an object with the surface character, visual weight, and permanence that ceramics offer, are difficult to achieve any other way.

References

[1] B. Kolbrek, “Development of horn loudspeakers before 1940,” Sep. 2014.

[2] K. T. Ulrich, S. D. Eppinger, and M. C. Yang, *Product Design and Development*, 6th ed. New York, NY: McGraw-Hill Education, 2016, ISBN: 978-0073404776.

[3] H. F. Olson, *Elements of Acoustical Engineering*, 1st ed. New York: D. Van Nostrand Company, Inc., 1940.

[4] J. H. Ginsberg, *Acoustics: A Textbook for Engineers and Physicists, Volume 1: Fundamentals*. Cham, Switzerland: Springer, 2018, ISBN: 978-3-319-56844-7. DOI: 10.1007/978-3-319-56845-4.

[5] J. Månsson and P. Nordbeck, *Flerdimensionell analys*, 1st. Lund, Sweden: Studentlitteratur AB, 2013, ISBN: 9789144080833.

[6] L. E. Kinsler, A. R. Frey, A. B. Coppens, and J. V. Sanders, *Fundamentals of Acoustics*, 4th ed. Wiley, 1999.

[7] T. Baasch and W. Qiu, “Bmen45 physical acoustics: Course lecture notes,” Internal course material via Canvas/LTH, Lecture notes for BMEN45, Department of Biomedical Engineering, Lund University (LTH), Lund, Sweden, Spring 2025.

[8] F. J. Fahy, *Foundations of Engineering Acoustics*. Oxford: Academic Press, 2000, Monograph, ISBN: 978-0-12-247665-5. DOI: 10.1016/B978-0-12-247665-5.X5000-8. [Online]. Available: https://www.sciencedirect.com/book/monograph/9780122476655/foundations-of-engineering-acoustics.

[9] T. Weideman. “Physics 9ha: Classical mechanics, Section 8.4: Coupled oscillators and normal modes,” University of California, Davis, Accessed: May 22, 2024. [Online]. Available: https://phys.libretexts.org/Courses/University_of_California_Davis/UCD%3A_Physics_9HA__Classical_Mechanics/8%3A_Small_Oscillations/8.4%3A_Coupled_Oscillators_and_Normal_Modes.

[10] N. S. Ottosen, M. Ristinmaa, and C. Ljung, *Hållfasthetslära: Allmänna tillstånd*, Swedish. Lund, Sweden: Studentlitteratur, 2007, ISBN: 978-91-44-05032-4.

[11] W. D. Callister Jr. and D. G. Rethwisch, *Fundamentals of Materials Science and Engineering: An Integrated Approach*, 6th. Hoboken, NJ: Wiley, 2020, ISBN: 978-1-119-68894-5.

[12] J. H. Ginsberg, *Acoustics: A Textbook for Engineers and Physicists, Volume 2: Applications*. Cham, Switzerland: Springer, 2018, ISBN: 978-3-319-61839-5. DOI: 10.1007/978-3-319-61840-1.

[13] B. Kolbrek, "Horn theory: An introduction," *audioXpress*, 2008, Available online at www.audioXpress.com.

[14] F. E. Toole, *Sound Reproduction: The Acoustics and Psychoacoustics of Loudspeakers and Rooms*, 3rd ed. New York, NY: Routledge, 2017, ISBN: 978-1-138-92136-8.

[15] D. Davis, E. Patronis, and P. Brown, *Sound System Engineering*, 4th ed. New York, NY: Routledge, 2013, ISBN: 978-0-240-81846-7. DOI: 10.4324/9780240818474.

[16] International Electrotechnical Commission, *IEC 60268-5: Sound system equipment — Part 5: Loudspeakers*, International Standard, Edition 3.0, Geneva, Switzerland, 2003.

[17] E. R. Geddes, "Acoustic waveguide theory," *Journal of the Audio Engineering Society*, vol. 37, no. 7, 1989.

[18] E. R. Geddes, "Acoustic waveguide theory revisited," *Journal of the Audio Engineering Society*, vol. 41, no. 6, 1993.

[19] J. E. Freehafer, "The acoustical impedance of an infinite hyperbolic horn," *Journal of the Acoustical Society of America*, vol. 11, no. 4, 1940.

[20] M. Batík, "OS-SE waveguide," AT-Horns, Tech. Rep., 2020, Available at https://at-horns.eu.

[21] D. Finkelnburg. "Clay minerals," Ceramic Arts Network, Accessed: Apr. 21, 2025. [Online]. Available: https://ceramicartsnetwork.org/ceramic-recipes/recipe/Clay-Minerals.

[22] J. Kaplan. "The whining stops here: A realistic look at clay bodies," Digitalfire Corporation, Accessed: Apr. 21, 2026. [Online]. Available: https://digitalfire.com/article/the+whining+stops+here%3A+a+realistic+look+at+clay+bodies.

[23] H. E. Exner and E. A. Giess, "Anisotropic shrinkage of cordierite-type glass powder cylindrical compacts," *Journal of Materials Research*, vol. 3, no. 1, pp. 122–125, 1988. DOI: 10.1557/JMR.1988.0122.

[24] C. Frayling, “Research in art and design,” *Royal College of Art Research Papers*, vol. 1, no. 1, pp. 1–5, 1993.

[25] I. Koskinen, J. Zimmerman, T. Binder, J. Redström, and S. Wensveen, *Design Research Through Practice: From the Lab, Field, and Showroom*. Waltham, MA: Morgan Kaufmann, 2011, ISBN: 978-0-12-385502-2. DOI: 10.1016/B978-0-12-385502-2.00015-8.

[26] BMS Speakers GmbH, *BMS 4550: 1" High Frequency Compression Driver Specifications*, Technical Data Sheet, BMS Speakers GmbH, Hannover, Germany, Apr. 2011. Accessed: May 22, 2024. [Online]. Available: https://bmsspeakers.com/fileadmin/bms-data/product_data_2011/compression_drivers_ferrite/bms_4550_2011-04_hf_compression_driver.pdf.

[27] BMS Speakers GmbH, *BMS 4550: 1" High Frequency Compression Driver Specifications*, Technical Data Sheet, 2022. Accessed: May 22, 2024. [Online]. Available: https://www.audiosciencereview.com/forum/index.php?attachments/compdriver-exit-angles-pdf.197929/.

[28] Keramik-Kraft. “Casting slip liquid stoneware anthracite W.” Product Technical Data, Accessed: May 22, 2024. [Online]. Available: https://www.keramik-kraft.com/en/Clay/Slips/Casting-Slips/casting-slip-liquid-stoneware-Anthracite-W-.html?sel=5.

[29] Cerama A/S. “Stentøjsstøbeler s20 hvid, 25 kg.” Danish, Cerama A/S, Accessed: May 11, 2026. [Online]. Available: https://cerama.dk/keramik/ler/stoebeler?ProductID=13320-S.

[30] Cerama A/S. “Råvarer.” Accessed: 2026-05-11, Cerama A/S, Accessed: May 11, 2026. [Online]. Available: https://cerama.dk/keramik/raavarer-mv/raavarer?ProductID=2892-1.

[31] Cerama High Temperature Products A/S, *Cerama automatik g20-20: Brugsanvisning*, Ver. 1.2, Cerama High Temperature Products A/S, Hvidovre, Danmark, Aug. 2017. [Online]. Available: cerama.dk.

[32] A. B. Williams, *Electronic Filter Design Handbook*, 1st ed. New York, NY: McGraw-Hill, 1981, ISBN: 9780070704305.

Appendix A – Derivation of the 1D Damped and Driven Oscillator Solution

The derivation presented in this section follows the derivations provided by Baasch and Qiu [7] in their course Physical Acoustics (BMEN45) at LTH. However, there have been some adaptations to the notation to create a simpler notation. Where possible additional references have been added.

A.1 Equation of Motion

Consider a mass m attached to a spring of stiffness k and a viscous damper with coefficient C. The displacement from equilibrium is denoted by $x(t)$ and the system is driven by an external force $F(t)$ as shown in fig. A.1

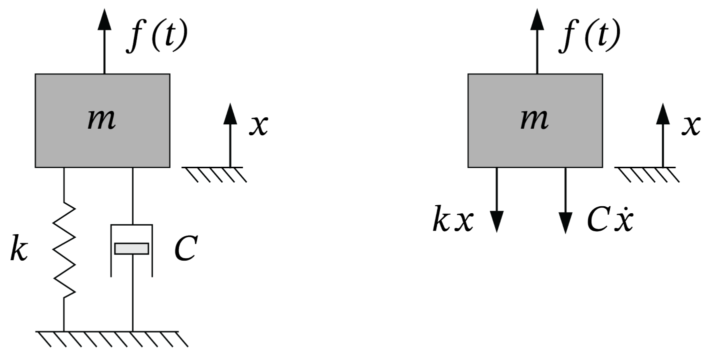

Figure A.1: Mass-spring system with free body diagram.

Setting up a force balance gives the equation of motion of the system

$$m\ddot{x}(t) = F(t) - kx(t) - C\dot{x}(t), \tag{A.1}$$

or equivalently

$$m\ddot{x}(t) + C\dot{x}(t) + kx(t) = F(t). \tag{A.2}$$

A.1.1 Complex formulation

To simplify the solution of the driven system, an equivalent complex-valued function $z(t)$ is introduced such that

$$x(t) = \Re\{z(t)\}. \tag{A.3}$$

[6] The equivalent complex equation with a harmonic driving force $Fe^{j\omega t}$ is then

$$m\ddot{z} + C\dot{z} + kz = Fe^{j\omega t}. \tag{A.4}$$

This approach allows for an algebraic solution rather than a trigonometric one.

The solution is decomposed in the standard homogeneous and particular solution z_H,z_P respectively as such

$$z(t) = z_H(t) + z_P(t). \tag{A.5}$$

A.1.2 Homogeneous solution

The homogeneous equation is

$$m\ddot{z}_H + C\dot{z}_H + kz_H = 0. \tag{A.6}$$

Using the exponential ansatz $z_H = e^{\lambda t}$ yields the characteristic equation

$$m\lambda^2 + C\lambda + k = 0. \tag{A.7}$$

Introducing the parameters

$$\omega_0^2 = \frac{k}{m}, \quad \gamma = \frac{C}{2m}, \tag{A.8}$$

the roots are

$$\lambda = -\gamma \pm \sqrt{\gamma^2 - \omega_0^2}. \tag{A.9}$$

For the underdamped case ($\gamma < \omega_0$), this becomes

$$\lambda = -\gamma \pm j\omega_d, \quad \omega_d = \sqrt{\omega_0^2 - \gamma^2}. \tag{A.10}$$

The solution can then be written as

$$z_H(t) = e^{-\gamma t}\left(Ae^{j\omega_d t} + Be^{-j\omega_d t}\right). \tag{A.11}$$

where A and B are constants determined from the initial conditions. This represents an oscillation at frequency ω_d with an exponentially decaying amplitude, corresponding to the transient response of the system.

A.1.3 Particular solution

To find the steady-state response, a solution with the same frequency as the driving force is required as such the ansatz

$$z_P(t) = \hat{z}e^{j\omega t} \tag{A.12}$$

is used. Substituting this into the equation of motion gives

$$\hat{z} = \frac{F}{-m\omega^2 + iC\omega + k}. \tag{A.13}$$

Rewriting in terms of ω_0 and γ yields

$$\hat{z} = \frac{F/m}{\omega_0^2 - \omega^2 + 2i\gamma\omega}. \tag{A.14}$$

The complex phasor $\hat{z}$ fully characterises the steady-state response: its magnitude determines the oscillation amplitude, while its phase determines the phase shift relative to the driving force.

The squared amplitude can easily be determined with the relation $|\hat{z}|^2 = zz^*$ as such

$$|\hat{z}|^2 = \left(\frac{F}{m}\right)^2 \frac{1}{(\omega_0^2 - \omega^2)^2 + (2\gamma\omega)^2}. \tag{A.15}$$

A.1.4 General solution

Combining both contributions, the full solution is

$$z(t) = e^{-\gamma t}\left(Ae^{j\omega_d t} + Be^{-j\omega_d t}\right) + \hat{z}e^{j\omega t}. \tag{A.16}$$

The physical displacement is obtained as

$$x(t) = \Re\{z(t)\}. \tag{A.17}$$

After a sufficiently long time, the transient term decays and the motion is dominated by the steady-state solution.

Appendix B – Plaster Preparation

Plaster used for slip casting is typically a beta hemihydrate. It can be prepared either by following manufacturer specifications or by using empirical methods such as the so-called “island method.” This method is less precise, but is commonly used in practice.

In the island method, water is first added to a container, and plaster is gradually sprinkled onto the surface. As the plaster absorbs water, small “islands” begin to form on the surface, as shown in fig. B.1. This indicates that the mixture is approaching the correct ratio.

The mixture is then left to soak briefly before being mixed, either by hand or mechanically. Care should be taken to avoid introducing air bubbles, as these can affect the quality of the mould surface. Adequate ventilation and dust protection are recommended when working with dry plaster.

Figure B.1: Formation of "plaster islands" during mixing, indicating that the plaster-to-water ratio is approaching saturation.

Appendix C – Project planning

C.1 Initial Calendar

The calendar below shows the initial project plan. It was revised several times as the project developed, primarily due to delays in 3D printing and the repeated casting attempts required for the OS horn.

20 # MARCH 26

MON	TUE	WED	THU	FRI	SAT	SUN
2	3	4	5	6	7	8
9	10	11	12	13	14	15
16	17	18	19	20	21 Determine geom-etry horn Use HornResp to verify geometry	22 CAD 3D models horns
23 Thesis start CAD 3D models plaster draft an-gles, parting line	24 Continue CAD plaster moulds Ask Olof about ceramics studio	25 Print 3D models for plaster moulds Write on report theory	26 Write on report theory Work on modal analysis	27 Continue modal analysis	28 Contact ancecho-ic chamber. Try to book a visit prior to testing	29
30 Post process 3D prints	31 Continue post processing 3D prints					

20 APRIL 26

MON	TUE	WED	THU	FRI	SAT	SUN
		1 3D print reference horns Continue theory	2 Pour plaster moulds?	3 Pour plaster moulds?	4 Start designing filter	5 Continue designing filter
6 Pour plaster moulds?	7 Pour plaster moulds?	8 Let moulds dry work on theory	9 Let moulds dry work on theory	10 Moving apartment	11	12
13 Remove plaster moulds from 3D prints and clean up moulds	14 Slipcast? Simulate filter in LtSpice?	15 Slipcast? Simulate filter in LtSpice? Order parts	16 Slipcast?	17 Post process casts?	18 Bisque fire?	19 Bisque fire?
20 Check for warping in casts	21	22 Assemble filter	23 Assemble filter	24 Test filter	25	26
27 Buffer day	28 Buffer day	29 Buffer day	30 Buffer day			

20 MAY 26

MON	TUE	WED	THU	FRI	SAT	SUN
				1 Buffer day	2	3
4 Test day?	5 Test day?	6 Test day?	7 Test day?	8 Test day?	9	10
11 Test day?	12 Test day?	13 Test day?	14 Test day?	15 Test day?	16 Write on report	17 Write on report
18 Process results	19 Process results	20 Process results	21 Write on report	22 Write on report	23 Write on report	24 Write on report
25 Write on report/ presentation	26 Write on report/ presentation	27 Write on report/ presentation	28 Write on report/ presentation	29 Write on report/ presentation	30 Finalise report	31

C.2 Project Logbook

Week 1 – 21 to 27 March

The week was primarily devoted to establishing the mathematical foundations of the horn profiles. Work began on the Kugelwellen and tractrix curves, deriving equations and verifying the mathematics using MATLAB. A key development was deriving a boundary constraint based on the exit angle of the compression driver, which became central to the parametrisation of the Kugelwellen profile. A meeting with Jože provided early guidance on the project direction. CAD work began in Creo towards the end of the week, with the Kugelwellen horn finalised. Following a discussion with Tsvetan, who noted his preference for oblate spheroid profiles, attention shifted towards investigating the mathematics and CAD of the oblate spheroid horn.

Week 2 – 28 March to 3 April

CAD work continued with the oblate spheroid horn, with several iterations on the parameters to arrive at a satisfactory geometry. All horn and mould CAD models were completed by the end of the week. Work then began on redesigning the horn models to account for wall thickness constraints identified during the mould design process, with air trap risks also reconsidered. Initial CAD work on the 3D printed mould shells began towards the end of the week.

Week 3 – 6 to 13 April

The oblate spheroid mould shells were finalised and sent for printing. Filter design work began in parallel, including derivation of the transfer function and verification in LTspice, with components ordered online. A meeting with Olof led to a significant redesign of the mould parts, simplifying the locking key geometry and introducing the fence-and-face approach for the 3D printed positives. An introduction to the ceramics studio at IKDC also took place this week. Revised mould designs for both the OS and Kugelwellen horns were sent for printing. The report structure was formally laid out and component orders were placed for the protection filter.

Week 4 – 14 to 21 April

The majority of this week was devoted to writing the theory chapter. The Kugelwellen horn 3D prints were received mid-week and post-processed. The first plaster casting attempt for the Kugelwellen mould took place on 20 April. Writing on the initial ideation and concept development began towards the end of the week.

Week 5 – 23 to 30 April

Writing continued on the concept development and CAD modelling chapters. Remaining OS horn 3D prints were received and post-processed. Plaster mould work for both the Kugelwellen and oblate spheroid horns continued across several days, with the final OS mould positive post-processed by the end of the week.

Week 6 – 1 to 9 May

Mould work was completed and the first slip casting attempts for both horns took place on 5 May. The Kugelwellen horn demoulded successfully. The OS horn exhibited internal defects on the first attempt, and a second casting was made with the mould rotated during pouring to try to achieve a more even wall. This also proved defective. A new batch of S20 slip was mixed, and an additional pour hole was drilled into the OS mould before a third casting attempt was made on 9 May.

Week 7 – 11 to 16 May

The third OS horn casting was demoulded and the green body cleaned up. The bisque-fired Kugelwellen horn was post-processed and a drill template was designed in CAD and 3D printed. Additional glaze was purchased. On opening the kiln, the OS horn was found to have exploded during bisque firing due to insufficient drying time. A fourth casting was made immediately and successfully demoulded and cleaned up by 14 May. The protection filter was built on 16 May.

Week 8 – 17 to 22 May

Writing progressed across the detailed design, concept realisation, and introduction chapters, with figures developed in parallel. The 3D printed PLA reference horns were received, sanded, and prepared. The OS horn was glazed and both ceramic horns had their mounting holes refined in preparation for acoustic measurements. All measurement equipment and materials were prepared by the end of the week.

Week 9 – 23 to 27 May

The acoustic measurement setup was assembled in the anechoic chamber on 23 May and measurements were taken on 24 May. The remainder of the week was spent on data analysis, writing the acoustical evaluation chapter, and beginning the discussion. All figures were completed on 27 May, followed by a final critical review of the report.

Appendix D – BMS-4550 2D CAD

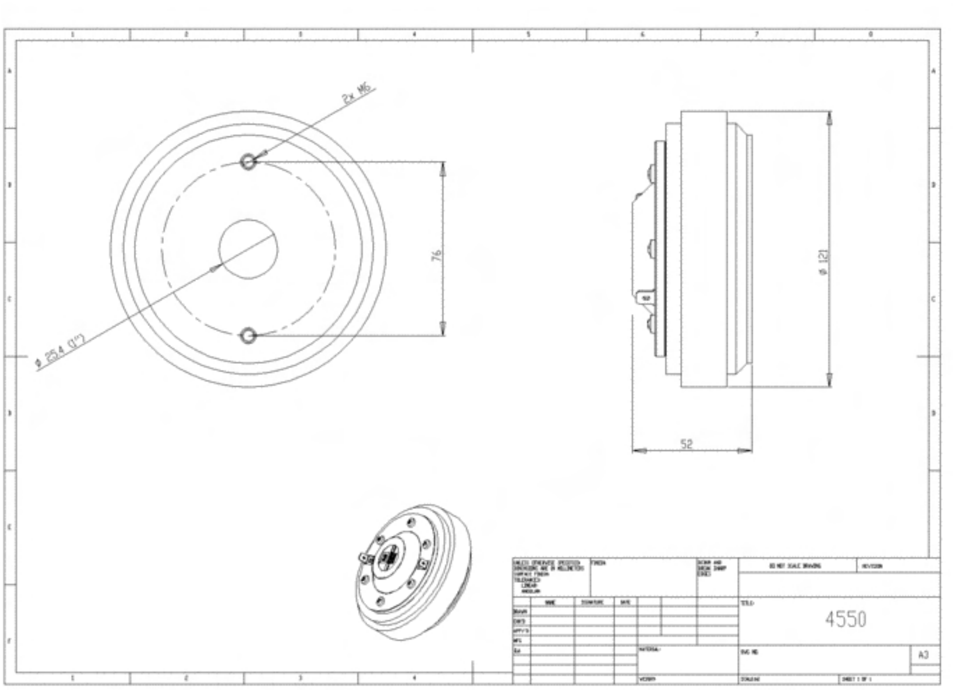

Figure D.1: BMS-4550 2D CAD Drawing

Appendix E – MATLAB CODE

E.1 Kugelwellen Compensating for Compression Driver Exit Angle

```
clear; clc;

%% Fixed parameters
c         = 343e3;          % mm/s
y_0       = 12.7;           % mm (1/2 inch throat)
ang       = 14;             % degrees
slope_tgt = tan(deg2rad(ang));

%% Solve for f_c
slope_fn = @(fc) compute_throat_slope(fc, c, y_0) -
    slope_tgt;
fc_sol   = fzero(slope_fn, [100, 5000]);

%% Derived constants
r_0 = c / (pi * fc_sol);
m   = 4 * pi * fc_sol / c;
h_0 = r_0 - sqrt(r_0^2 - y_0^2);

%% Print results
fprintf('f_c = %.4f Hz\n',   fc_sol);
fprintf('r_0 = %.4f mm\n',   r_0);
fprintf('m   = %.6f mm^-1\n', m);
fprintf('h_0 = %.6f mm\n',   h_0);
fprintf('Verification: throat angle = %.4f deg\n', ...
        rad2deg(atan(compute_throat_slope(fc_sol, c, y_0))
            ));

%% Helper function
function s = compute_throat_slope(fc, c, y_0)
    r0 = c / (pi * fc);
    if y_0 > r0
```

```
        s = NaN; return
    end
    m   = 4 * pi * fc / c;
    h_0 = r0 - sqrt(r0^2 - y_0^2);
    s   = m * h_0 * sqrt(r0^2 - y_0^2) / (y_0 * (1 - m*h_0));
end
```

E.2 Oblate Spheroid with Clothoid

```
clear; clc;

%% Parameters
r0           = 12.7;    % throat radius (mm)
alpha0       = 14;      % throat half-angle (deg)
alpha_H      = 30;      % horizontal coverage half-angle (deg)
alpha_V      = 20;      % vertical coverage half-angle (deg)
A            = 40;      % clothoid scale parameter (mm)
L_target     = 100;     % total horn depth (mm)
target_angle = deg2rad(130);     % clothoid exit angle (rad)

%% Solve for OS length and generate profiles
L_H = fzero(@(L) maxDepth(L, r0, alpha0, alpha_H, A, target_angle) - L_target, [1 500]);
L_V = fzero(@(L) maxDepth(L, r0, alpha0, alpha_V, A, target_angle) - L_target, [1 500]);

[z_H, r_H] = fullProfile(r0, alpha0, alpha_H, L_H, A, target_angle);
[z_V, r_V] = fullProfile(r0, alpha0, alpha_V, L_V, A, target_angle);

%% Plot
figure; hold on;
plot(z_H,  r_H, 'b-', 'LineWidth', 2, ...
     'DisplayName', sprintf('Horizontal \\alpha = %d ', alpha_H));
plot(z_H, -r_H, 'b-', 'LineWidth', 2, 'HandleVisibility', 'off');
plot(z_V,  r_V, 'r-', 'LineWidth', 2, ...
```

```
    'DisplayName', sprintf('Vertical \\alpha = %d ', alpha_V));
plot(z_V, -r_V, 'r-', 'LineWidth', 2, 'HandleVisibility', 'off');
xlabel('Axial distance z (mm)');
ylabel('Radius r (mm)');
legend('Location', 'northwest');
grid on; axis equal;

%% OS profile
function r = OS(z, r0, alpha0, alpha)
    r = sqrt(r0^2 + 2*r0*z*tan(deg2rad(alpha0)) + z.^2*tan(deg2rad(alpha))^2);
end

%% OS + clothoid profile
function [z_out, r_out] = fullProfile(r0, alpha0, alpha, L, A, target_angle)
    z_os = linspace(0, L, 2000);
    r_os = OS(z_os, r0, alpha0, alpha);

    % Match slope and curvature at junction
    dz   = z_os(2) - z_os(1);
    dr   = gradient(r_os, dz);
    d2r  = gradient(dr,   dz);
    ang  = atan(dr(end));
    curv = d2r(end) / (1 + dr(end)^2)^(3/2);

    % Integrate clothoid from junction
    s     = linspace(0, A*sqrt(abs(target_angle - ang))*3, 5000);
    kappa = curv + s/A^2;
    theta = ang + cumtrapz(s, kappa);
    idx   = find(theta >= target_angle, 1);

    z_out = [z_os, z_os(end) + cumtrapz(s(1:idx), cos(theta(1:idx)))];
    r_out = [r_os, r_os(end) + cumtrapz(s(1:idx), sin(theta(1:idx)))];
end

%% Helper: total depth of profile
function d = maxDepth(L, r0, alpha0, alpha, A, target_angle)
    [z, ~] = fullProfile(r0, alpha0, alpha, L, A, target_angle);
    d = max(z);
```

```
end
```

Appendix F – Passive Filter

To protect the BMS 4550 compression driver from low-frequency content below its recommended crossover frequency of 800 Hz, a passive second-order Butterworth high-pass filter was designed and built. A Butterworth filter places its poles to produce a maximally flat pass-band with no ripple, rolling off at −12 dB per octave for a second-order design [32].

F.0.1 Realisation for BMS 4550

The filter was implemented as the passive RLC circuit shown in fig. F.1.

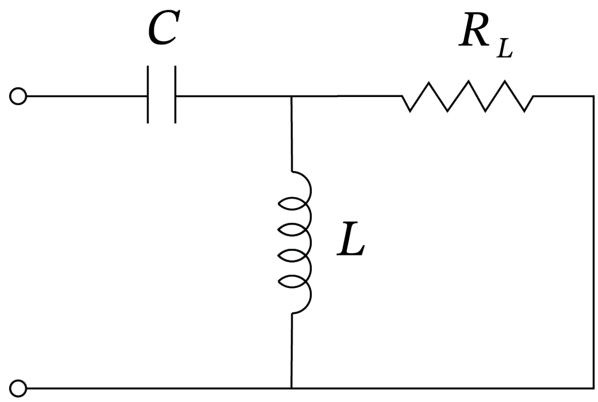

Figure F.1: Passive second-order Butterworth high-pass filter. Component values L and C set the cut-off frequency $\omega_c = 1/\sqrt{LC}$ and the Butterworth damping condition.

The transfer function of this circuit is:

$$H(s) = \frac{s^2}{s^2 + \frac{s}{R_L C} + \frac{1}{LC}}. \tag{F.1}$$

Matching the denominator to the second-order Butterworth polynomial gives:

$$\begin{cases} \sqrt{2}\,\omega_c = \dfrac{1}{R_L C} \\ \omega_c^2 = \dfrac{1}{LC}. \end{cases} \tag{F.2}$$

Taking $R_L = 8\,\Omega$ as the nominal impedance of the BMS 4550 — an approximation, since driver impedance varies with frequency — yields $L = 2.25\,\text{mH}$ and $C = 17.6\,\mu\text{F}$. Standard component values of $L = 2.2\,\text{mH}$ and $C = 18\,\mu\text{F}$ were verified in LTspice to give adequate performance. The filter was assembled using point-to-point wiring and mounted to a plywood sheet, and verified audibly prior to use in the acoustical evaluation.